



**NUST COLLEGE OF  
ELECTRICAL & MECHANICAL  
ENGINEERING**

**DESIGN OF A MICRO AERIAL VEHICLE  
THROUGH BIO-INSPIRED KINEMATICS USING  
HIGH SPEED CAMERA**

PROJECT REPORT

DE-41 (DME)

*Submitted by*

DANIYAL ZIAFAT  
MALIK HUZAIFA SAEED  
MUHAMMAD USAMA  
MUHAMMAD TAJDAR IRFANI

**BACHELORS  
IN  
MECHANICAL ENGINEERING  
YEAR  
2023**

**PROJECT SUPERVISOR**

DR IMRAN AKHTAR  
DR ZAFAR ABBAS BANGASH

**NUST COLLEGE OF  
ELECTRICAL AND MECHANICAL ENGINEERING  
PESHAWAR ROAD, RAWALPINDI**

---

## DECLARATION

We hereby declare that no portion of the work referred to in this Project Thesis has been submitted in support of an application for another degree or qualification of this or any other university or other institute of learning. If any act of plagiarism is found, we are fully responsible for every disciplinary action taken against us depending upon the seriousness of the proven offence, even the cancellation of our degree.

---

## COPYRIGHT STATEMENT

- Copyright in text of this thesis rests with the student author. Copies (by any process) either in full, or of extracts, may be made **only** in accordance with instructions given by the author and lodged in the Library of NUST College of E&ME. Details may be obtained by the Librarian. This page must form part of any such copies made. Further copies (by any process) of copies made in accordance with such instructions may not be made without the permission (in writing) of the author.
  - The ownership of any intellectual property rights which may be described in this thesis is vested in NUST College of E&ME, subject to any prior agreement to the contrary, and may not be made available for use by third parties without the written permission of the College of E&ME, which will prescribe the terms and conditions of any such agreement.
  - Further information on the conditions under which disclosures and exploitation may take place is available from the Library of NUST College of E&ME, Rawalpindi.
-

---

## **ACKNOWLEDGEMENTS**

In the name of Allah, the Most Merciful and the Most Beneficial. It is the great blessing of Allah Almighty, that He has given us the power to accomplish this project as well as our degree with our heads high. First of all, we would like to thank our parents and teachers for their good wishes and prayers. We would like to thank our supervisors, Dr Imran Akhtar, Dr Zafar Abbas Bangash for their assistance, as, without their help, this project can't be completed. We would also like to thank all faculty members for their assistance in our project development directly or indirectly.

---

---

## **ABSTRACT**

This paper addresses the design and development of a bio-inspired micro unmanned aerial vehicle (MAV) based on the flight kinematics of dragonflies. Dragonflies exhibit exceptional flight capabilities, including hovering, agile maneuvering, and gliding, making them an intriguing model for MAV design. The objective of this research is to study the kinematics of dragonfly flight, analyze their aerodynamics, and design a flapping mechanism that replicates their unique wing motion. Video analysis and kinematics techniques were employed to measure important parameters such as flapping angles, phase angles, and angle of attack. Aerodynamics analysis utilized potential flow analysis to examine the overall aerodynamic characteristics of the wing. The design of the flapping mechanism focused on accurately reproducing natural wing motion observed in insects. By combining these efforts, this study aims to provide valuable insights into the flight mechanics of dragonflies and contribute to the development of bio-inspired MAVs

---

# TABLE OF CONTENTS

<b>Declaration and Copyright Certificate .....</b>	<b>2</b>
<b>Acknowledgements .....</b>	<b>3</b>
<b>Abstract.....</b>	<b>4</b>
<b>Table of Contents .....</b>	<b>6</b>
<b>List of Figures.....</b>	<b>10</b>
<b>List of Tables .....</b>	<b>11</b>

## **Chapter 1**

### **Introduction**

1.1 Background.....	12
1.2 Problem Statement.....	12
1.3 Objectives.....	13
1.4 SDGs.....	13

## **Chapter 2**

### **Literary Review**

2.1 Flight Characteristics of Dragon fly .....	15
2.1.1 Hovering .....	16
2.1.2 Forward Flight .....	16
2.1.3 Accelerated Flight.....	16
2.1.4 Gliding .....	17
2.1.5 Backward Flight.....	17
2.2 Methods for measuring wing kinematics.....	17
2.2.1 High Speed Video.....	18
2.2.2 3D Photogrammetry.....	18
2.3 Flapping Wing Aerodynamics.....	19
2.3.1 Leading Edge Vortices .....	19
2.3.2 Unsteady Effects: LEV Stability .....	20
2.3.3 Unsteady Effects: Rotational Circulations.....	21

2.3.4 Unsteady Effects: Wake Capture.....	22
2.3.5 Tandem Wing Configurations .....	23

## Chapter 3

### Kinematics

3.1 Tool Selection.....	25
3.2 Analysis on Python.....	26
3.2.1 Video Preprocessing .....	26
3.2.2 Object Tracking .....	26
3.2.3 Parameters Extraction.....	27
3.2.4 Calibration .....	27
3.3 Kinematic Parameters.....	28
3.3.1 Flapping Angles.....	28
3.3.2 Angle of Attack.....	29
3.3.3 Phase Angle .....	29
3.3.4 Stroke Plane .....	29
3.4 Mapped coordinates of wings.....	30
3.4.1 Forewing Data .....	31
3.4.2 Hindwing Data.....	32
3.5 Kinematics Parameter Calculations.....	33
3.5.1 Flap Angle Calculations .....	33
3.5.2 Angle of Attack Calculations.....	33
3.5.3 Phase Angle Calculations .....	34
3.6 Governing Equations.....	35

## **Chapter 4**

### Aerodynamics

4.1 Concept of Potential Flows.....	36
4.2 Classification of Potential Flows .....	37
4.3 Unsteady Vortex Lattice Method.....	38
4.4 MATLAB Implementation .....	42
4.5 Aerodynamics Loads .....	43

## **Chapter 5**

### Design of Flapping Mechanism

5.1 Parameters.....	45
5.1.1 Radius of Crank.....	45
5.1.2 Length of Connecting Rod.....	45
5.1.3 Slider.....	46
5.1.4 Connecting Rod .....	46
5.1.5 Rocker.....	46
5.2 Derivation of Position, Velocity, and Acceleration.....	47
5.3 Derivation of Flapping Angle and Angle of Transmission .....	49
5.3.1 Angle of Transmission.....	51
5.3.2 Flapping Angle .....	52
5.3.3 Design Parameter Calculations.....	52
5.4 Mechanism Design on solidworks .....	55
5.4.1 Prototype I .....	56

5.4.2 Prototype II .....	56
5.5 Design Validation .....	56

## **Chapter 6**

### Results

6.1 Flight Data .....	57
6.2 Factors Affecting Lift Coefficient .....	59
6.3 Force Coefficients.....	60
6.4 Flight Performance .....	61

## **Chapter 7**

### Conclusion

7.1 Conclusion .....	63
----------------------	----

<b>References.....</b>	<b>64</b>
------------------------	-----------

## LIST OF FIGURES

Figure 1: 3D Photogrammetry Setup .....	18
Figure 2: Dragonfly Stroke cycle.....	23
Figure 3: Kinematic parameters in Cartesian Plane.....	29
Figure 4: Analysis on Software.....	31
Figure 5: Forewing flap change with time .....	32
Figure 6: Hindwing location with time.....	33
Figure 7: Quadrilateral panels.....	39
Figure 8: Time marching steps .....	40
Figure 9: Wake Vortex Matrix.....	41
Figure 10: Matlab Results .....	43
Figure 11: Slider Crank Mechanism .....	47
Figure 12: Mechanism Part 1 .....	49
Figure 13: Mechanism Part II .....	51
Figure 14: Prototype I .....	56
Figure 15: Prototype II.....	57
Figure 16: Flapping Angle .....	59
Figure 17: Coefficient of Lift.....	60

# LIST OF TABLES

Table 1: Forewing XY Coordinates with time.....	32
Table 2: Hindwing XY coordinates with time.....	33
Table 3: Parameter Values .....	55
Table 4: Design Parameters .....	57
Table 5: Flight Data .....	58

---

# CHAPTER 1: INTRODUCTION

## 1.1 Background

Aerial robotics have made significant progress in recent years, particularly in the development of unmanned aerial vehicles (UAVs). Engineers are making use of biomimicry, designs inspired by nature, to improve adaptability and maneuverability of UAV designs. The amazing flight ability of dragonflies has grabbed the interest of scientists trying to explore new pathways in aerial robots. This final-year project intends to develop a Micro Aerial Vehicle (MAV) based on dragonfly flight kinematics. High-speed cameras will be used to record and analyze the delicate movements of dragonflies in flight, providing significant information on wing motion, stroke patterns, and body dynamics. This data will be used to build a bio-inspired kinematic model to optimize the MAV's wing mechanism.

The amazing flight ability of dragonflies has grabbed the interest of scientists trying to explore new pathways in aerial robots. The goal of this final-year project is to create a MAV based on dragonfly flight kinematics. High-speed cameras will be utilized to record and analyze dragonfly flying movements, providing valuable information on wing motion, stroke patterns, and body dynamics. This information will be utilized to create a bio-inspired kinematic model to optimize the wing mechanism of the MAV.

## 1.2 Problem Statement

Aerial robotics have made amazing advances in recent years, allowing construction of UAVs for many applications. Conventional UAV designs, on the other hand, typically lack the maneuverability, stability, and energy economy exhibited by the flies in nature. This makes achieving optimal flight performance and adaptability in UAVs a substantial problem. The issue at hand is the requirement for a more efficient and nimble UAV design that mimics dragonfly flight capabilities. Existing UAV designs use fixed-wing or rotor-based propulsion systems, limiting their maneuverability and flexibility in complex situations. To circumvent these restrictions, a bio-inspired technique based on dragonfly flying kinematics is offered.

The project intends to address this issue by developing a MAV with bio-inspired mechanics and high-speed camera technologies. The primary goal is to record and analyze dragonfly flight motions to extract essential flight metrics such as wing motion, stroke patterns, and body dynamics. The effective use of the bio-inspired kinematic model will help to enhance aerial robotics by providing a new paradigm for UAV design. It will pave the way for more efficient and nimble UAVs capable of precisely navigating complicated surroundings and adapting to changing conditions.

### **1.3 Objectives**

The project aims to achieve several objectives. Firstly, it involves the extraction of kinematic parameters of dragonfly flight from high-speed camera video recordings. This data will provide valuable insights into the wing motion, stroke characteristics, and flight performance of dragonflies. Secondly, based on the extracted kinematic values, a flapping wing mechanism will be developed. This mechanism will mimic the wing motion of dragonflies and enable the creation of a bio-inspired flapping wing system. Thirdly, an aerodynamics analysis will be conducted to ensure the generation of lift and optimize the performance of the flapping wing mechanism. This analysis will involve studying the airflow around the wings and assessing the forces involved in lift production. Lastly, utilizing the knowledge gained from the previous objectives, a bio-inspired flapping wing MAV will be designed.

### **1.4 Sustainable Development Goals**

Our research is focused on the creation and deployment of bio-inspired MAVs, which are miniature unmanned aerial vehicles meant to mimic the flight of insects, birds, and other creatures. These micro-UAVs outperform standard drones in difficult situations, where they can travel effectively, operate quietly, and hover with precision.

One of the primary applications of micro-UAVs is in surveillance and monitoring tasks. They are invaluable in scenarios where human access is limited or dangerous, such as offshore oil rigs or remote wilderness areas. Deploying micro-UAVs for pipeline inspections, ship traffic

monitoring, or dam inspections provides critical data that can prevent accidents and ensure safety. Micro-UAVs have the potential to revolutionize crop production in the agriculture sector. They let farmers monitor crops, detect signs of stress or illness, and intervene in time to save crop loss. Furthermore, these UAVs may collect data on soil conditions, weather patterns, and other elements influencing crop development, allowing farmers to make informed planting and harvesting decisions.

The significance of our project extends beyond its immediate applications. It is consistent with several United Nations Sustainable Development Goals (SDGs), including SDG 9 (industry, innovation, and infrastructure), SDG 8 (economic growth and decent work), and SDG 2 (end hunger and promote sustainable agriculture). By increasing agricultural productivity, we contribute to SDG 8 by fostering economic growth and generating employment opportunities. Simultaneously, we address SDG 2 by improving food security, ensuring access to nutritious food, and promoting sustainable agricultural practices. Through the development and utilization of Bio-inspired MAVs, our project actively works towards a more sustainable future by addressing global challenges outlined in the SDGs.

## **CHAPTER 2: LITERARY REVIEW**

The literature review focuses on the existing research related to bio-inspired kinematics and its application in the design and fabrication of MAVs. The research on dragonflies can be divided into two phases. The first phase comprises research before the early 1990s, when researchers like Azuma [1], May [2] and Wakeling [3] set the groundwork for the study of dragonfly flight aerodynamics. The researchers used cameras to record photographs of dragonflies in flight and then analyzed flight characteristics, such as the angle of attack, flapping angles, and motions of the two independent pair of wings during various flying maneuvers. The aerodynamic forces generated by the wings were measured experimentally, allowing researchers to investigate the relationship between the movement of the wings and the force generated [4].

The second phase of dragonfly research started in the late 1990s and continues to this day. During this period, a great amount of work has been done to investigate the biological importance of dragonfly behavior and how these contribute to mechanisms enhancing lift and thrust. Researchers such as Thomas [5], Wang [6], and Sun [7] have made significant contributions, revealing the effects of wing-wing interaction. Researchers such as Thomas [5], Wang [6], and Sun [7] have made significant contributions, revealing the effects of wing-wing interaction. These studies have demonstrated that the two independent pair of wings not only produce the aerodynamic load needed for prolonged flapping flight but also improve aerodynamic efficiency through wing-wing interactions. The advancements in high-speed videography, computational modeling, and mechanical modeling have greatly contributed to the rapid progress in understanding dragonfly aerodynamics. The subsequent section of this paper sheds light on the existing research on Bio-inspired kinematics and their application in the design and fabrication of MAVs.

### **2.1 Flight Characteristics of Dragonfly**

Flapping flight, characterized by structural movement and unsteady fluid dynamics, presents a more intricate challenge compared to fixed-wing flight. Dragonflies are equipped with two independent pairs of wings that are capable of beating in phase or out of phase. They can

effortlessly glide, hover, accelerate rapidly, and sustain forward flight, making them adept at evading predators through various flight modes.

### **2.1.1 Hovering**

Hovering, a distinctive behavior observed in dragonflies, is accomplished by maintaining a precise phase angle of 180 degrees between the movements of their wing pairs. Through meticulous coordination of wing motions in an antiphase configuration, dragonflies generate equal lift and thrust forces, allowing them to remain stationary in mid-air while observing their environment or targeting prey. During hovering flight, the wing pairs execute a figure-of-eight pattern within the stroke plane, which is nearly vertical. Each wing pair beats independently at significant angles of attack. This flight pattern induces unsteady aerodynamic flow patterns in the surrounding air. When averaged over a complete wing stroke, dragonflies can sustain a lift force two to three times their body weight. Studies have reported wing lift coefficients ( $C_L$ ) exceeding 2.3 during hovering flight [9].

### **2.1.2 Forward Flight**

In forward flight, the phase angle between wing motions typically ranges from 54 to 100 degrees with the hindwing leading the forewing. This specific wing coordination results in enhanced efficiency and generates greater thrust compared to single-flapping wings with dragonflies reaching speeds of up to 100 body lengths per second.

### **2.1.3 Accelerated Flight**

During accelerated flight, dragonflies synchronize their wing pairs such that there is 0° phase difference. This arrangement optimizes thrust and lift generation, allowing dragonflies to reach speeds of up to 13.4 m/s. This method of flying, however, demands a substantial amount of power and can only be sustained for limited periods of time. As a result, dragonflies often engage in fast flight when pursuing prey or lifting off, when a significant thrust force and high lift are required. This adaptation allows dragonflies to swiftly respond to their surroundings and efficiently navigate their environment during critical moments.

### **2.1.4 Gliding**

When dragonflies engage in gliding, they extend their wings and adjust the phase angles based on the prevailing airflow conditions. This stretching of the wings during gliding helps them optimize flight efficiency by reducing energy expenditure. Dragonflies dynamically adjust their phase angles to maintain a balance between gliding and controlled flapping, allowing them to cover longer distances with minimal energy consumption.

### **2.1.5 Backward Flight**

The research of Bode-Oke[10] uncovers that dragonflies have the capability to engage in backward flight, which differs from their conventional forward flight. This backward flight mode involves distinct changes in the kinematics and aerodynamics of the dragonflies' wing movements. To achieve backward flight, dragonflies make specific adjustments to their kinematics. They accomplish this by tilting their stroke plane towards their bodies, altering the orientation of their wing movements. This reorientation allows dragonflies to redirect the generated force in a way that enables them to fly in the opposite direction. By modifying the kinematics in this manner, dragonflies can sustain backward flight for extended periods.

## **2.2 Methods for Measuring Wing Kinematics**

Measurement of wing kinematics has remained a difficult task for scientists for many years. The frequency at which dragonflies flap their wings is so high that it is typically impossible for a person to see individual wing strokes. In addition, the wing simultaneously translates, rotates, and deforms, making it much more challenging to measure any parameter precisely. In addition, the forewings, and the hindwings of dragonfly flap at different phase angles which requires the use of precise measurement techniques.

### **2.2.1 High-Speed Video**

Early attempts to quantify insect wing kinematics relied on the use of a single camera to capture high-speed film of their flight. In the absence of digital imaging technology, combining detailed quantitative data from multiple cameras was extremely challenging.

Consequently, the early methods were restricted to utilizing information from a single imaging plane. Nonetheless, researchers employing this approach were able to make significant initial approximations of basic dragonfly body and wing kinematics. For instance, Ruppell conducted extensive studies, capturing over 12,000 meters of film while recording high-speed videos of various dragonflies and damselflies flying out of a box [11]. This wealth of data allowed him to estimate various kinematic parameters such as flight velocity, wingbeat frequency, wingbeat phasing, upstroke/downstroke ratio, stroke amplitude, and even the angle of attack.

### 2.2.2 3D Photogrammetry

Three-dimensional photogrammetry, as shown in Figure 1, is the most recent approach for measuring kinematics and deformations of insect wings. This concept is based on a method that has been well-validated and is used in a number of applications, including video game development and cinematography. Three-dimensional photogrammetry involves employing projective geometry to determine the three-dimensional coordinates of points captured by a spatially calibrated multi-camera system. This technique is computationally intensive but offers unparalleled accuracy and resolution in measuring wing kinematics including turning flights [16]. Moreover, it provides sufficient space for handling of free-flying subjects.

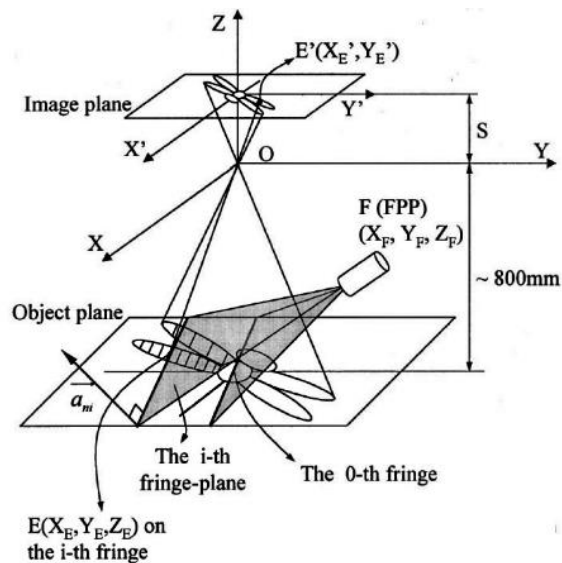


Figure 1: 3D Photogrammetry Setup

## **2.3 Flapping Wings Aerodynamics**

Dragonflies possess remarkable flight abilities due to the intricate mechanisms involved in the aerodynamics of their flapping wings. The wings of dragonflies exhibit a complex geometry characterized by camber, twist, and corrugation. These features are crucial for generating lift and minimizing drag. The flapping motion, comprising translational and rotational components, enables precise control over lift and thrust. This exceptional flight performance of dragonflies is due to interactions between wing shape, kinematics, and vortex dynamics. By thoroughly analyzing the aerodynamics of dragonfly wings, we can gain valuable insights for designing and optimizing flapping-wing MAVs. Therefore bio-inspired designs hold the potential to enhance maneuverability and efficiency in small-scale robotic flyers.

### **2.3.1 Leading Edge Vortices**

At low Reynolds numbers, the boundary layer and flow separation characteristics in flapping-wing flights differ from those of larger fixed-wing aircraft. Studies by Ellington and others revealed that insect wings exhibited a delayed stall behavior, attributed to a large region of separated flow at the leading edge [13]. This separation bubble was found to increase the effective camber and thickness of the wing, improving aerodynamic performance near stall conditions. These early investigations laid the foundation for the discovery of a crucial aerodynamic mechanism in low Reynolds number flapping wings: the leading-edge vortex (LEV). Rapid changes in the angle of attack or translational acceleration at high angles of attack induced flow separation, resulting in the formation of a vortex that increased lift production by creating a low-pressure zone. The presence of the LEV in insect flight proved highly advantageous, with lift values up to 200 percent higher than in stalled conditions. While LEVs can also appear on high Reynolds number airfoils undergoing rapid pitching motions, they are quickly shed into the wake, limiting their benefits. In contrast, the presence of the LEV in insect flight is more advantageous due to its ability to remain attached throughout each half-stroke. This sustained attachment results in a continuous

generation of high-velocity flow and low-pressure zones, significantly enhancing lift production. LEV plays a crucial role in the aerodynamic performance of flapping-wing systems, demonstrating the unique capabilities of insects in generating lift and enabling agile flight in low Reynolds number regimes.

### **2.3.2 Unsteady Effects: LEV Stability**

The mechanism responsible for maintaining the attachment of LEVs to the upper surface of insect wings remains a subject of ongoing debate. One potential factor implicated in this process is axial flow, which involves the flow of air from the wing root to the wingtip. Axial flow is believed to contribute to LEV stability by removing vorticity from the vortex core, preventing it from growing too large and detaching. This phenomenon, known to be crucial for delta-wing aircraft at high Reynolds numbers, may also play a role in insect wings despite their lower Reynolds numbers.

However, the theory of axial flow's involvement in LEV stability has been challenged by Birch and Dickinson, who conducted experiments on model fruit fly wings with partial chordwise fences to obstruct axial flow [14]. Surprisingly, they found that blocking axial flow at the leading edge did not decrease LEV stability or force production significantly. Instead, they observed a 25 percent decrease in aerodynamic force when fences were mounted at the trailing edge. This suggests that axial flow may not be the primary mechanism responsible for LEV attachment in fruit fly wings. Nevertheless, it remains uncertain whether this conclusion applies to the wings of larger insects at higher Reynolds numbers. Birch and Dickinson proposed an alternative explanation, suggesting that a combination of the downward induced flow caused by the tip vortex and the downwash due to lift production forms a momentum jet that inhibits the strength of the LEV and prevents detachment.

These conflicting findings highlight the complexity of understanding LEV attachment and the role of axial flow in insect wing aerodynamics. Further research is necessary to elucidate the mechanisms governing LEV stability and attachment in different insect species, especially at varying Reynolds numbers. Advancements in experimental techniques and

computational modeling may contribute to a better understanding of these intricate flow phenomena.

### **2.3.3 Unsteady Effects: Rotational Circulations**

Initially, studies on insect wing aerodynamics primarily focused on quantifying the quasi-steady aerodynamic forces during the translational phase of the wing stroke. During this phase, the rotational periods that occurred during stroke reversal were considered mainly as kinematic adjustments to align the wing at the appropriate angle of attack for the next half-stroke. However, it was soon recognized that the wing's rotation during stroke reversal must generate circulation, which contributes significantly to the overall lift produced during a wing stroke [15].

Subsequent investigations revealed that this rotational circulation had a much greater impact than initially anticipated, leading to significant force peaks at the end of each half-stroke. It became evident that the timing of the wing rotation plays a crucial role in the generation of lift throughout the flapping cycle. Figure 2 illustrates the effects of different rotational timings on lift production. In Column A, advanced rotation occurs entirely at the end of a half-stroke. In this case, rotational and translational circulation act in the same direction, reinforcing each other. Consequently, significant lift peaks are observed just before stroke reversal. On the other hand, Column C depicts delayed rotation, where rotation takes place at the beginning of a half-stroke. Since the rotational circulation opposes translational circulation, large negative rotational lift peaks are observed, resulting in a substantial reduction in the force on the wing. Rotational timing can also fall between these two extremes, and symmetrical rotation has been found to produce only a slight reduction in overall lift compared to advanced rotation.

These findings highlight the importance of understanding the rotational phasing employed by insects in any kinematic study. It is now evident that the rotation of the wing, which occurs during periods of translational deceleration, acceleration, or both, plays a significant role in

generating lift. The specific timing and coordination of rotational and translational circulation have a profound effect on the overall lift production during a flapping cycle. Further research in this area is crucial for a comprehensive understanding of insect wing aerodynamics and the optimization of flight performance.

#### **2.3.4 Unsteady Effects: Wake Capture**

When the insect wing completes a half-stroke and starts moving in the opposite direction, it encounters its wake, leading to several significant effects. One of these effects is the induced flow within the wake, which plays a role in limiting the growth of the LEV and maintaining its attachment to the wing surface. The presence of the wake itself can also increase lift on the wing through a mechanism called wake capture. If the wing begins the half-stroke with a positive angle of attack in the case of advanced rotation, the incoming wake generates a positive lift force as it passes over the wing. Conversely, if the wing rotation is delayed and the angle of attack is negative at the start of the half-stroke, the wake generates a negative lift. The forces arising from wake capture in these scenarios are depicted in the lower panels of columns A and C in Figure 2 and are represented by an open circle. Notably, the timing of the wake capture lift peak remains independent of rotational phasing, but its sign and magnitude are not fully determined.

Understanding the interaction between the wing and its wake is crucial in comprehending the complex aerodynamics of insect flight. The induced flow within the wake potentially aids in maintaining the attachment and stability of the leading-edge vortex. Furthermore, the phenomenon of wake capture contributes to the overall lift produced during the wing's motion. The timing of the wing's rotation, whether advanced or delayed, influences the direction and magnitude of the lift generated through wake capture. These findings underscore the intricate interplay between the wing, its wake, and the resulting aerodynamic forces.

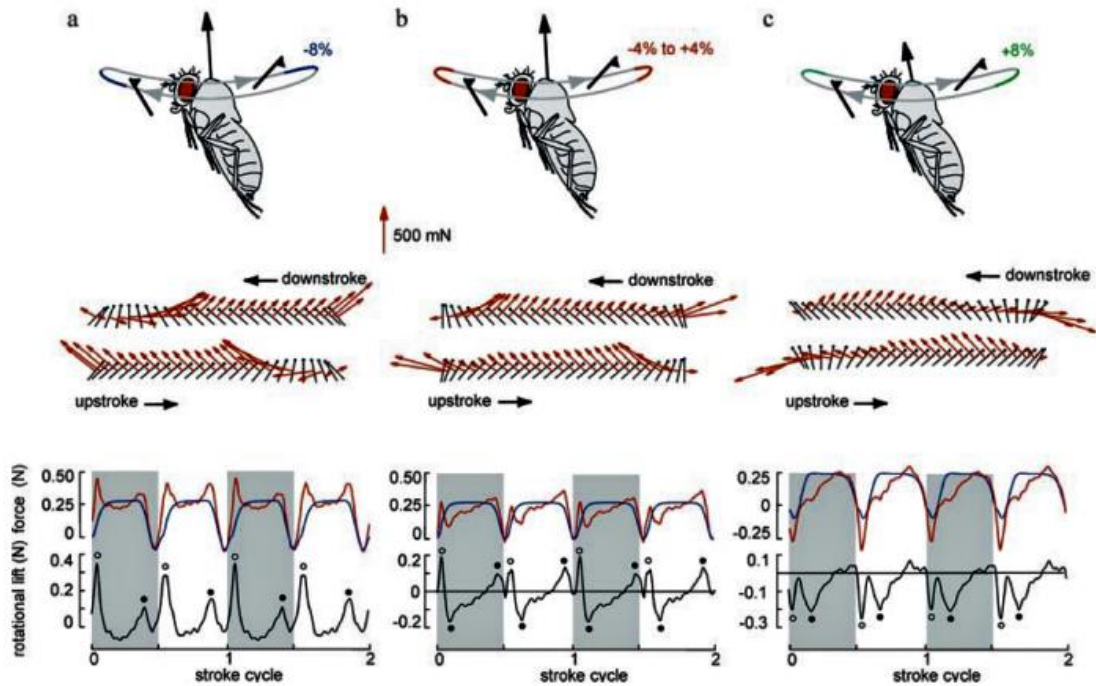


Figure 2: Insect Stroke cycle

### 2.3.5 Tandem Wing Effects

Understanding the intricate aerodynamics of dragonfly flight presents an additional challenge due to their use of tandem wings. Unlike insects with a single pair of wings, each wing of a dragonfly interacts not only with its wake but also with the wake generated by the other wings. Dragonflies possess the remarkable ability to independently control each of their four wings, enabling various kinematic combinations of wing stroke phasing.

During the straight flight, dragonflies have been observed to flap their forewings and hindwings approximately 180 degrees out-of-phase with each other during cruising. However, they flap their wings in-phase during periods of high acceleration. Computational fluid dynamics (CFD) studies have demonstrated that adjusting the phasing of the wings leads to significant changes in the performance of a dragonfly model [15]. In-phase flapping

results in high thrust production but lower lift efficiency, while 90 and 180 degree out-of-phase flapping generates lower thrust but significantly higher lift efficiency. The decrease in propulsive efficiency during counter-stroking flight is attributed to the hindwing extracting energy from the wake created by the forewing.

Flow visualization studies conducted on tethered and free-flying dragonflies have provided insights into the aerodynamic phenomena associated with different wing stroke phasing. During counter-stroking flight, a LEV is observed on the forewing during the downstroke, while the flow remains attached during the forewing upstroke and throughout the entire hindwing stroke. In contrast, in-phase stroking results in greater flow separation and the presence of a single large, attached LEV spanning both the fore- and hindwings. The significant size of this attached vortex is likely responsible for the exceptionally high lift coefficients observed.

These findings emphasize the importance of considering the complex interaction between the wings and their wakes in dragonfly flight. The ability of dragonflies to independently control their wings and adjust the phasing allows them to optimize their aerodynamic performance for different flight conditions. Continued investigations, combining experimental techniques and numerical simulations, are necessary to unravel the detailed mechanisms underlying the aerodynamics of tandem-winged insects like dragonflies. Such studies can provide valuable insights into the design principles and efficiency of biological flight systems and inspire advancements in biomimetic aerial vehicles.

## CHAPTER 3: KINEMATICS

The video analysis and kinematics section aim to extract precise parameters from high-speed videos of dragonfly flight and derive comprehensive kinematic equations to describe intricate wing motion. By utilizing advanced computer vision techniques and tracking algorithms, detailed measurements of flapping angles, phase angles, and angles of attack were obtained, providing crucial insights into the kinematics of dragonfly flight. This analysis significantly contributes to our understanding of the flight dynamics, maneuverability, and aerodynamic performance of dragonflies, serving as a valuable foundation for bio-inspired MAV design and optimization.

### 3.1 Tool Selection

Many tools are available for video processing tasks, which offer powerful capabilities for image and video processing tasks. To select a suitable tool, we compared MATLAB and Python. Although both offered a variety of options for processing images and videos, however, certain factors influenced the choice of Python for video preprocessing in this project.

Python, with its extensive libraries such as OpenCV and NumPy, offers a wide range of tools and functions specifically designed for image and video processing tasks. These libraries offer efficient and optimized algorithms for tasks like contrast enhancement, image stabilization, object tracking, and calibration. Python's rich ecosystem and community support make it an ideal choice for developing complex video processing pipelines. Moreover, Python's integration with other scientific and data analysis libraries, such as pandas and matplotlib, offers seamless data handling and visualization capabilities. This integration enables the project to leverage the extracted parameters from video analysis for

further data analysis, statistical modeling, and visualization, enhancing the overall understanding of dragonfly flight dynamics.

Considering these factors, Python emerges as a favorable choice for video preprocessing in this project. Its comprehensive libraries, ease of use and integration with other scientific aligns well with the requirements of extracting precise measurements from high-speed videos of dragonfly flight.

## **3.2 Analysis on Python**

In the analysis of dragonfly flight kinematics, several steps are undertaken to measure and understand the movement of the wings. These steps include video preprocessing, calibration, object tracking, and parameter extraction. Wing and body lengths are then measured by annotating and calculating distances between key points. These analysis techniques provide valuable insights into the kinematics of dragonfly flight, aiding in the understanding of flight dynamics and aerodynamic performance.

### **3.2.1 Video Preprocessing**

Video preprocessing plays a critical role in preparing the captured frames for subsequent analysis. It involves applying various techniques to enhance the quality and accuracy of the frames. The provided code incorporates two key preprocessing techniques. Firstly, a grayscale conversion is performed using the `cv2.cvtColor()` function, which transforms the frames from color BGR to grayscale. This conversion simplifies the subsequent analysis by reducing the dimensionality of the frames while preserving important intensity information. Secondly, Gaussian blur is applied to the frames using the `cv2.GaussianBlur()` function. This blurring process effectively diminishes noise and irregularities, leading to smoother frames. By improving the visibility of wing features and reducing noise interference, these preprocessing steps significantly enhance the accuracy of subsequent tracking and parameter extraction, ultimately facilitating a more precise analysis of dragonfly flight.

### **3.2.2 Object Tracking**

Object tracking is a vital component of video analysis, enabling the continuous monitoring of wing motion in video sequences. The provided code employs contour detection and moment calculation techniques to extract essential wing features such as centroid coordinates and wing angles. Contour detection is accomplished using the `cv2.findContours()` function, which identifies the boundaries of connected components, representing the wing shape. By computing the moments of each contour with the `cv2.moments()` function, crucial information about the distribution of pixel intensities and the wing's centroid is obtained. These tracking techniques provide accurate and reliable data for subsequent analysis, allowing for a comprehensive understanding of dragonfly flight dynamics.

### **3.2.3 Parameter Extraction**

Once the wings have been successfully tracked, the subsequent step involves extracting key kinematic parameters that provide a characterization of the dragonfly's flight. The provided code focuses on three significant parameters: flapping angles, phase angles, and the angle of attack. In the code, measurement of flapping angles was made by analyzing wing motion with respect to a reference axis or predefined anatomical landmarks. While estimation of the angle of attack was made by analyzing the pitching motion of the wing and calculating the angle formed with the horizontal axis, which represents the axis of the fluid flow. Extracting these parameters through the video analysis process yields quantitative measurements of wing motion, enabling a comprehensive characterization of the dragonfly's flight kinematics.

### **3.2.4 Calibration**

First, suitable reference objects with known dimensions, such as a ruler or calibration grid, were selected and placed within the field of view during video recording. Using tracker software, the positions of these reference objects were manually annotated in the video frames, allowing for their tracking throughout the sequence. The known dimensions of the reference objects were measured using conventional techniques, providing ground truth measurements in desired units, such as millimeters. By comparing the known dimensions

with the corresponding pixel values of the annotated video frames, a calibration factor was derived, enabling the conversion of pixel values to physical units. With the calibration factor established, the wing length and body length of the dragonfly were measured by manually annotating the wingtips and anterior/posterior points in each frame. The Euclidean distances between these annotated points were calculated in pixel units and then converted to physical units using the calibration factor. This incorporation of reference measurement and calibration into the analysis workflow allowed for accurate and quantitative measurements of the dragonfly's wing length and body length, facilitating a deeper understanding of their morphology and kinematics.

### **3.3 Kinematic Parameters**

To ensure an accurate understanding and calculation of flapping wing motion, it is crucial to define key parameters. The parameters of interest for our project are stroke plane, flapping angles, phase angles, and angles of attack. Figure 3 provides a graphic representation of the flapping motion of a dragonfly's wings. The figure depicts a relative coordinate system, denoted as  $x'y'z'$ , which is derived by rotating the absolute coordinate system,  $xyz$ , by an angle  $\alpha$ . Within this relative coordinate system, the stroke angle  $\alpha$ , stroke amplitude  $\beta$ , and angle of attack  $\delta$  are defined.

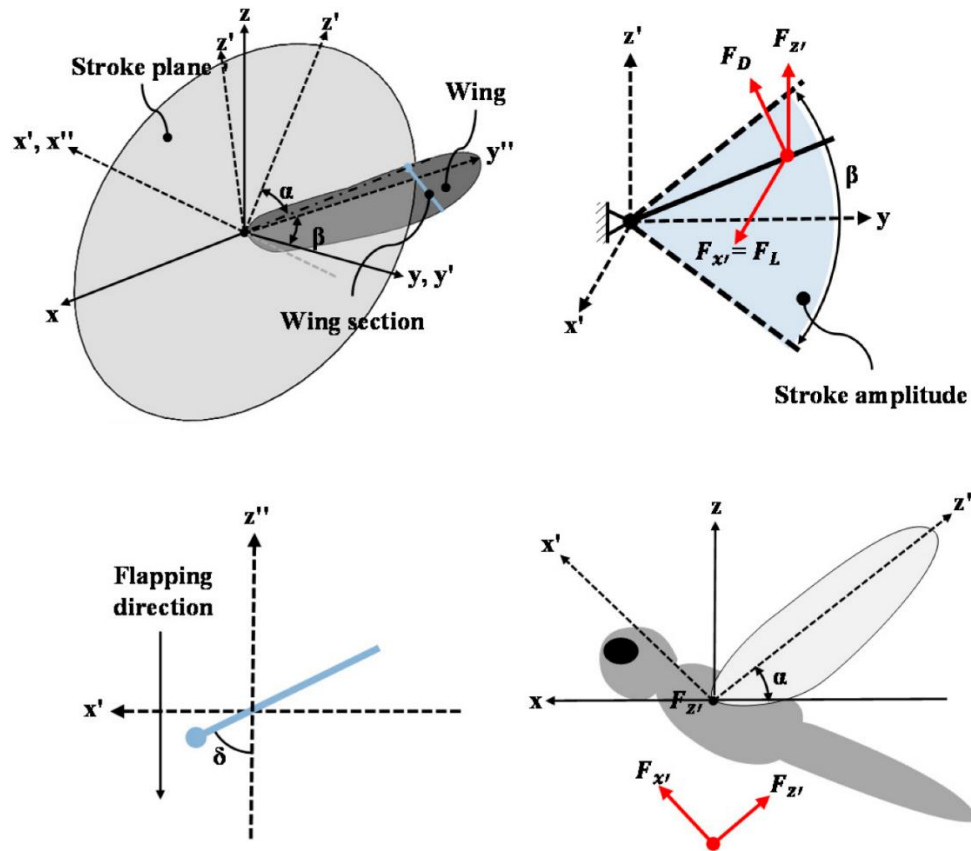


Figure 3: Kinematic parameters in Cartesian Plane

### 3.3.1 Flapping Angles

The flapping angle refers to the angle at which the wings of a dragonfly or any other flapping-wing mechanism are positioned during their motion. It represents the deviation of the wings from their resting or neutral position. The flapping angle is typically measured as the angular displacement of the wings relative to a reference point, such as the body axis or the horizontal plane. It plays a crucial role in generating lift and thrust during flight.

### 3.3.2 Angle of Attack

The angle of attack refers to the angle between the chord line of the airfoil and the free stream. For a dragonfly, the angle of attack represents the orientation of its wings with respect to the air as it moves. Angle of attack is an important aerodynamic parameter that can significantly affect the aerodynamic characteristics of flight. A higher angle of attack can increase lift but may also introduce additional drag and contribute to stall. Controlling the

angle of attack allows the dragonfly to regulate its flight performance, maneuverability, and stability.

### **3.3.3 Phase Angle**

The phase angle refers to the angular relationship or phase difference between two different moving components within a mechanism. In the context of a dragonfly's flapping-wing mechanism, the phase angle typically describes the relative timing or synchronization between the flapping motion of the forewing and hindwing. The phase angle determines the coordination between the wings, ensuring an efficient and effective flapping pattern for flight.

### **3.3.1 Stroke Plane**

The stroke plane of a dragonfly refers to the specific path or plane along which its wings move during flapping. It represents the trajectory followed by the wings as they go through the different phases of the wingbeat cycle. The stroke plane plays a crucial role in generating lift and propulsion, enabling the dragonfly to achieve stable and controlled flight.

## **3.4 Mapped Coordinates of Wings**

Capturing of wing tip coordinates was done by taking a solid dark point on leading edge of both forewing and hindwing. Ideally, the coordinates of wing movement should have been captured automatically by the code for each frame but due to the limitation of video quality and our knowledge of computer vision, we extracted coordinate of wings separately for each frame. The coordinates were captured in the x-y direction with respect to time. This was done for 2 flaps of both forewing and hindwing which comprised approximately 30-40 frames. Each frame's coordinates were carefully recorded and documented.

In Figure 4, the leading edge of the forewing is traced in red, while the leading edge of the hindwing is traced in blue. These traces visually represent the captured wing tip coordinates. Subsequently, the obtained data was manipulated, and various calculations and measurements were performed to extract the kinematics of the dragonfly, allowing for a comprehensive understanding of its wing movements and aerodynamic characteristics.

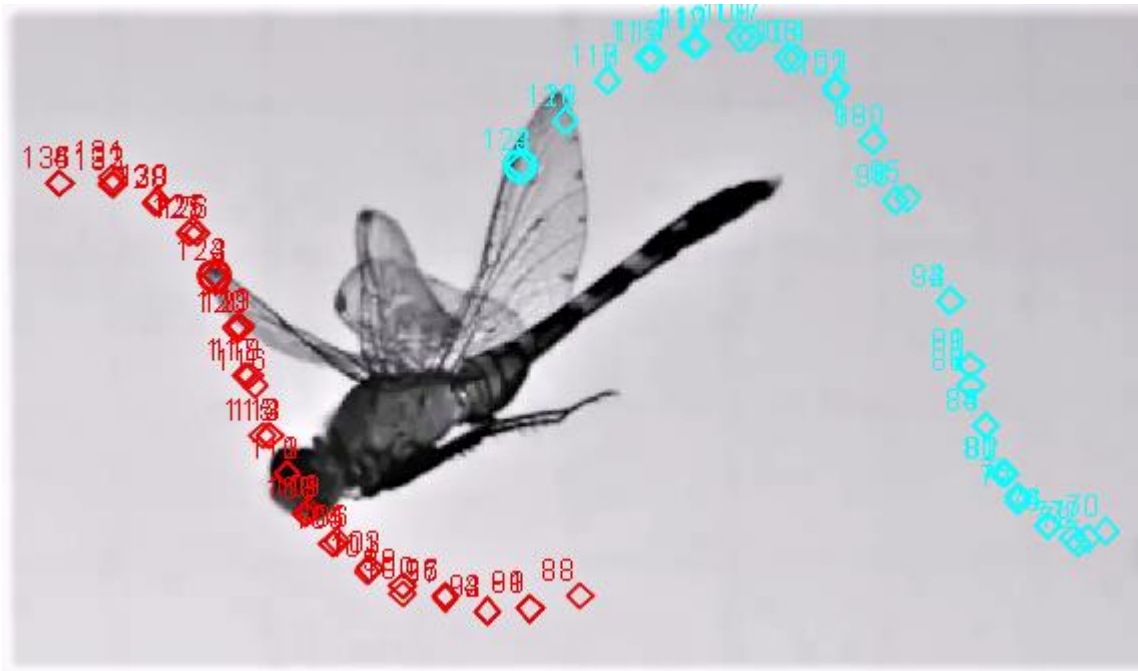


Figure 4: Analysis on Software

### 3.4.1 Forewing Data

Black solid point on forewing was tracked and marked manually for each frame and the respective x-y coordinate for the point with respect to time were also noted down. This process was done for 30-40 frames which cover a complete single flap. Figure 5 shows the position of front wing reference point in x-y plane.

Time	X	Y
2.9333	1.9532	-0.4448
2.9667	1.6437	-0.5221
3.0000	1.6437	-0.5221
3.0333	1.6437	-0.5221
3.0667	1.3730	-0.5415
3.1000	1.3730	-0.5415
3.1333	1.3730	-0.5415
3.1667	1.1023	-0.4448
3.2000	1.1023	-0.4448
3.2333	1.1023	-0.4641

3.2667	0.8315	-0.3868
3.3000	0.8315	-0.3868
3.3333	0.8315	-0.4254
3.3667	0.5995	-0.2901
3.4000	0.6188	-0.2707
3.4333	0.6188	-0.2707
3.4667	0.3868	-0.1160
3.5000	0.3868	-0.1160
3.5333	0.4061	-0.0967
3.5667	0.2127	0.0774
3.6000	0.2127	0.0774
3.6333	0.2321	0.0967

Table 1: Forewing XY Coordinates with time

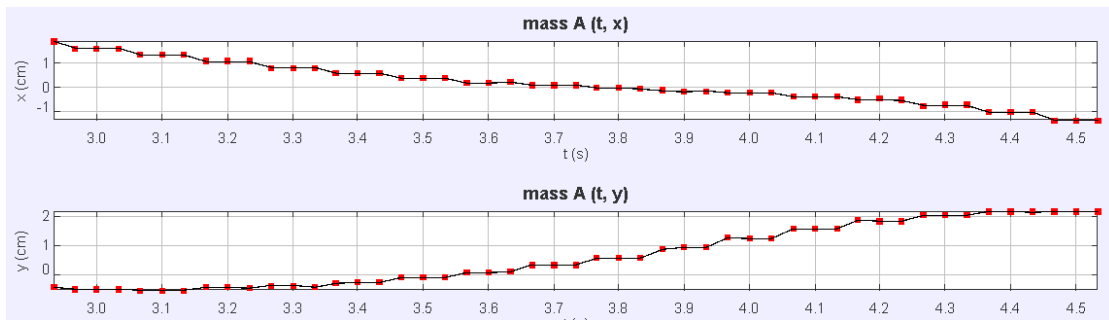


Figure 5: Forewing flap change with time

### 3.4.2 Hindwing Data

Black solid points on Hindwing were tracked and marked manually for each frame and the respective x-y coordinate for the point with respect to time were also noted down. This process was done for 30-40 frames which cover a complete single flap. Figure 6 shows the position of hind wing reference point in x-y plane.

Time	X	Y
2.3333	5.2986	-0.0387
2.3667	5.0859	-0.0774
2.4000	5.1826	-0.0774
2.4333	5.1246	-0.1160
2.4667	4.9312	0.0000
2.5000	4.9312	0.0000
2.5333	4.9312	0.0000
2.6000	4.7378	0.1934
2.6333	4.7378	0.1547

2.6667	4.6412	0.3287
2.7000	4.6412	0.3287
2.7333	4.6605	0.3287
2.7667	4.5251	0.6382
2.8000	4.5251	0.6382
2.8333	4.5251	0.6382
2.8667	4.4284	0.8896
2.9000	4.4284	0.8896
2.9333	4.4284	0.8896
3.6000	0.2127	0.0774
3.6333	0.2321	0.0967

Table 2: Hindwing XY coordinates with time.

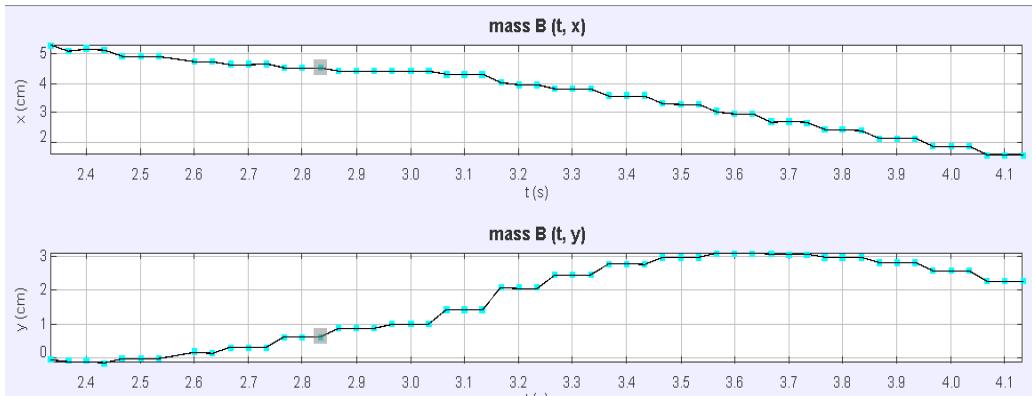


Figure 6: Hindwing location with time

### 3.5 Kinematic Parameters Calculations

To analyze the flight dynamics and wing motion characteristics of the dragonfly, precise calculations of key kinematic parameters are essential. This section focuses on the calculation of three significant parameters: flap angle, angle of attack, and phase angle. These parameters provide valuable insights into the wing movements and temporal evolution of the dragonfly's flight. By carefully extracting and transforming the wingtip coordinates, right-angled triangles are formed to determine the relationships between vertical and horizontal distances. Trigonometric calculations, such as tangent or inverse tangent, are then employed to derive the specific values for each parameter. Through these calculations, a deeper understanding of the dragonfly's flight behavior can be achieved, contributing to the broader knowledge of insect flight mechanisms.

### **3.5.1 Flap Angle Calculations**

To determine the flap angle of the dragonfly's wing, a series of steps are utilized. Initially, the coordinates (x, y) of the wingtip are obtained by tracking positions in each frame. These coordinates are then transformed relative to a reference axis, which is commonly specified as the line joining the anterior and posterior locations of the dragonfly. These transformed coordinates are then used to create a right-angled triangle, with the triangle's sides representing the vertical distance (y-axis) and horizontal distance (x-axis) of the wingtip position. The flap angle is the angle adjacent to the y-axis and can be found using basic trigonometry. The tangent of the flap angle can be determined by dividing the vertical distance of the wingtip position by its horizontal distance.

### **3.5.2 Angle of Attack Calculations**

To calculate the angle of attack of the dragonfly's wing, some manipulations are required. The coordinates (x, y) of the leading and trailing edge of wing positions are extracted from the tracking data. These coordinates are then transformed relative to each other. Transformed coordinates are now used to create a right-angled triangle, with the vertical distance representing one side and the horizontal distance representing the other. The angle of attack is the angle adjacent to the vertical axis and can now be calculated in the same way that flapping angles were calculated.

### **3.5.3 Phase Angle Calculation**

To determine the phase angle, which represents the relative position of each wing during the flapping cycle, a mathematical approach was developed. Initially, the coordinates (x, y) of the leading edge of both the forewing and hindwing wings are extracted from the tracking data. These coordinates were plotted on a graph with the y-axis representing the location of the wings and the x-axis representing time (in radians). The phase angle in radians can now be determined by analyzing the difference in the starting point of the waveform. Through these calculations, valuable insights into the wing motion characteristics and flight dynamics

of the dragonfly can be obtained, contributing to a deeper understanding of its flight behavior.

### 3.6 Governing Equations

From the calculations of flap angle, angle of attack, and phase angle, we can derive sinusoidal waveforms that represent the motion of the dragonfly's flapping wings. These sinusoidal waveforms provide valuable information for modeling the pitch and heave motions of the wings. The heave motion describes the up-and-down translatory movement of the wings, while the pitch motion represents the rotation of wings around horizontal axis. By analyzing the sinusoidal waveforms derived from the angle measurements, we can formulate governing equations that describe these motions. The heave motion can be expressed by the equation:

$$h(t) = h_0 \cos(2\pi ft)$$

where  $h(t)$  represents the heave displacement at time  $t$ ,  $h_0$  is the maximum amplitude of the heave motion,  $f$  is the flapping frequency, and  $t$  is time. Heave amplitude can be found by multiplying the sine of flapping angle with the distance up to the mean chord of the wing. Heave amplitude also plays a crucial role in determining the Strouhal number for the flight.

Similarly, the pitch motion can be described by the equation:

$$\Phi(t) = \Phi_0 \sin(2\pi ft)$$

where  $\Phi(t)$  represents the pitch displacement at time  $t$ ,  $\Phi_0$  is the amplitude of the pitch motion,  $f$  is the flapping frequency, and  $t$  is time. Pitch amplitude is the angle of attack for a wing, as pitch motion is responsible for producing the angle between the chord of wing and the free stream.

These governing equations provide a mathematical representation of the pitch and heave motions of the dragonfly's wings during flight. They allow us to quantitatively analyze and

model the complex wing kinematics, enabling a deeper understanding of the aerodynamic forces, lift generation, and maneuverability exhibited by the dragonfly.

## **CHAPTER 4: AERODYNAMICS**

The aerodynamic analysis of the flapping wing micro aerial vehicle is conducted using an analytical approach, focusing on the resolution of potential flows. This method offers advantages in terms of simplicity and computational efficiency compared to CFD techniques. By assuming that the flow remains attached to the wing throughout the flapping motion, we obtain time-accurate solutions, considering changes in circulation distribution, time-dependent velocity potential, and the movement of the circulatory wake. While potential flow analysis may lack the precision of full CFD simulations, it provides valuable insights into the

overall aerodynamic characteristics of the wing, allowing for the identification of critical design parameters and facilitating parametric studies.

## 4.1 Concept of Potential Flow Methods

To model the flapping wing problem using potential flow theory, several assumptions are made. Firstly, a 2D flow is assumed. It is a good approximation keeping in mind the typical aspect ratios of insect wings. Additionally, a flat plate model is employed since the thickness and camber of insect wings are usually negligible compared to the chord length. Furthermore, the flow is assumed to be inviscid so the effects inside the boundary layer are ignored. This combined with the inherent irrotationality condition in potential flow, simplifies the governing equation to the Laplace equation where the complex potential's Laplacian is zero.

To use this equation, the following assumptions must be made. certain conditions must be maintained throughout the flow. These include subsonic and incompressible flow, irrotationality, and inviscid behavior. The preservation of irrotationality requires the flow to remain attached everywhere, ensuring that no flow separation occurs. This leads to definition of Laplace equation based on continuity equation:

$$\nabla \cdot U = 0$$

The resolution of the Laplace equation relies on finding elementary solutions, known as singularities, which are then combined using the principle of superposition to construct the overall flow field. To obtain a solution for the Laplace equation, a pair of boundary conditions is required. The first condition is impermeability, which mathematically involves canceling the normal component of velocity at the surface. The second condition, known as the Kutta condition, is applicable in the case of lifting bodies and requires the flow to smoothly detach at the trailing edge.

In summary, modeling the flapping wing problem using potential flow theory involves making assumptions about the flow, such as 2D flow, flat plate simplification, inviscid behavior, and irrotationality. The Laplace equation is then used to solve for the flow field by

combining singularities. Boundary conditions, including impermeability and the Kutta condition, further constrain the solution. These assumptions and conditions enable us to analyze the aerodynamic behavior of the flapping wing micro aerial vehicle within the framework of potential flow theory.

## **4.2 Classification of Potential Flows**

Potential flow methods can be classified based on several factors. The first classification is related to the steadiness or unsteadiness of the flow, which is determined by the boundary conditions imposed. Another classification criterion is the discretization of the domain and the types of singularity used, including sources, doublets, vortices, or high-order elements generated by computer algorithms. A third differentiation is based on the wake model employed. The wake, which can significantly affect the aerodynamic properties of the wing in unsteady flow, can be represented as a free wake that moves with respect to the local flow velocity or as a simpler flat wake that is convected by the free stream without deformation.

Another classification criterion considers the thickness of the body. For thin bodies, computational resources can be saved by modeling the airfoil using only its camber line. Singularities, such as vortices to generate circulation and doublets to represent thickness, are placed along the camber line based on thin airfoil theory. However, for relatively thin airfoils with a thickness not exceeding 30% of the chord, the influence of thickness on aerodynamic forces is minimal in non-stationary flow, and it can be neglected.

In the scope of this thesis, the focus is on the aerodynamics of a flapping flat plate. To analyze this problem, the unsteady vortex lattice method (UVLM) will be utilized. The UVLM approach combines unsteady potential flow theory with a lattice discretization of the wing to capture the effects of vortex shedding and wake dynamics. By employing the UVLM method, the thesis aims to investigate the aerodynamic characteristics and performance of the flapping flat plate in a comprehensive manner.

### 4.3 Unsteady Vortex Lattice Method

UVLM is a valuable tool for solving 3D potential flow problems and accurately representing lifting surfaces. In this method, the lifting surfaces and the wake are modeled using vortex ring elements. Each vortex ring is composed of a quadrangle, which consists of four vortex segments of constant and equal intensity. The solution of the unsteady vortex lattice method is obtained through a time-marching algorithm. At the beginning of the resolution, the vortex rings of the wake are shed freely at the trailing edge of the wing. Subsequently, they deform with respect to the local flow in the case of a free wake model or are convected by the free stream in the case of a flat wake model. In our model, we employ the flat wake model.

To discretize the lifting surfaces, quadrilateral panels are employed. Each panel is associated with a vortex ring, as shown in Figure 7. The impermeability condition is imposed at the collocation point of each panel, where the vortex rings attached to a lifting panel, known as bound vortices, are positioned. To implicitly satisfy the Kutta condition, the leading segment of the vortex ring is placed on the panel's quarter-chord line. The collocation points are located at the center of the three-quarter chord line of the corresponding panel. A normal vector, denoted as  $n$ , is defined at each collocation point, and the vorticity, is assigned to each segment following the right-hand rule, as depicted in Figure 7.

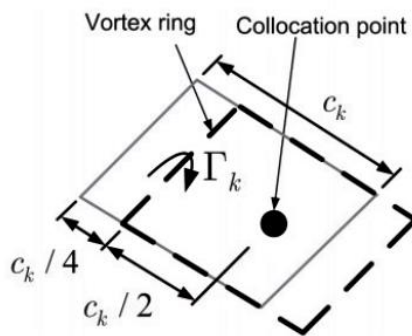


Figure 7: Quadrilateral panels

The wake consists of a vortex sheet that is generated at the trailing edge of the wing and sheds freely, resulting in wake vortices. These vortices are usually referred to as wake vortices. The vortex ring model for the initial time steps is illustrated in Figure 8.

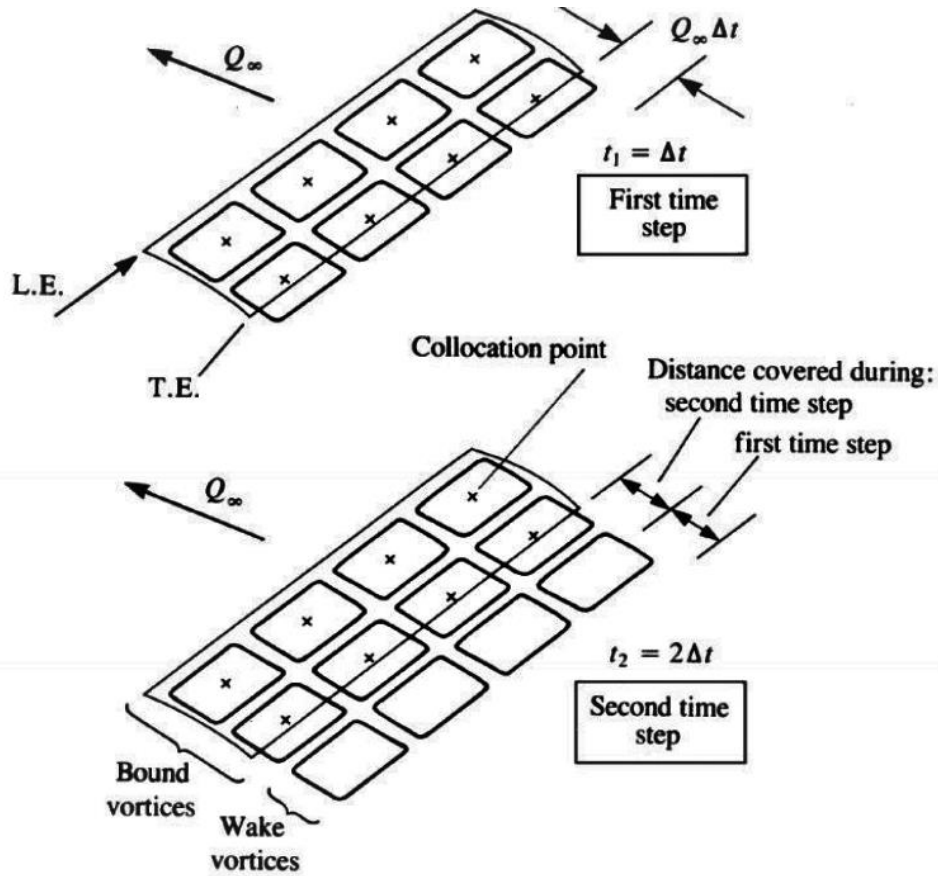


Figure 8: Time marching steps

At the discrete time step  $n+1$ , the impermeability condition is enforced at each collocation point, leading to the determination of the vorticity for each vortex ring. Mathematically, this condition is expressed by canceling the normal component of the local velocity at the collocation point of each panel. Consequently, the sum of the contributions to the normal velocity at the collocation point is zero. The velocity induced by the vortex rings is calculated for each panel using the Biot-Savart law.

$$\mathbf{q}_{kl} = \oint_{C_j} \frac{d\mathbf{s}_j \times \mathbf{r}_{kl}}{4\pi r_{kl}^3}$$

To reduce computation time, only the influence of the wake panels near the wing is considered. This approximation is justified as the influence of distant wake panels diminishes

significantly. In the codes developed for this thesis, only the portion of the wake that is smaller than five times the chord length is considered for computing the wake influences matrix. The strength of the new shed wake vortex is set equal to the strength of the bound vortex located at the trailing edge in the previous time step. It is important to note that the vorticity remains unchanged due to the absence of dissipation, as governed by Kelvin's theorem.

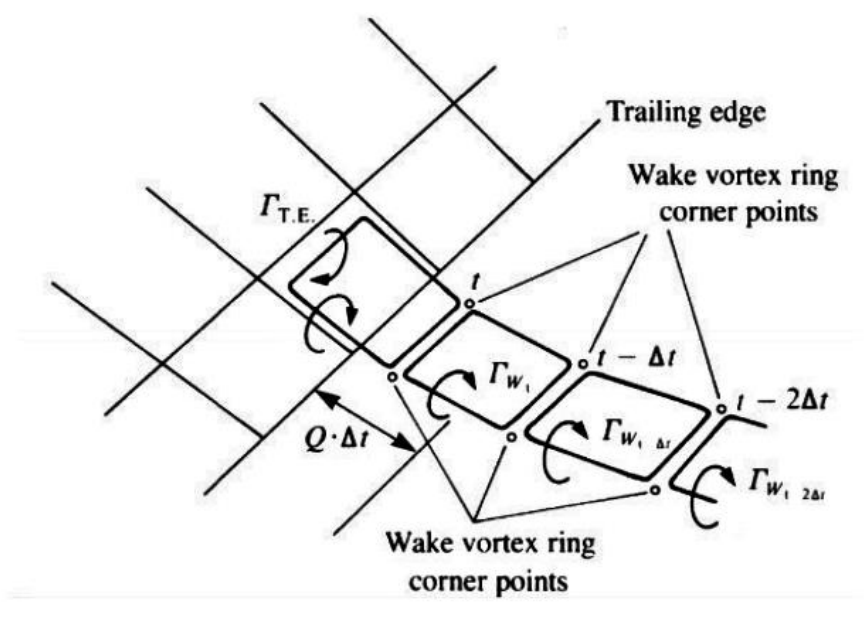


Figure 9: Wake Vortex Matrix

In the case of a flat wake, as shown in Figure 9, all the wake rings are simply transported with the flow in a straight line, requiring no further computations. Finally, by employing the impermeability condition and the equations governing the wake, all elements of the problem are known, except for the strength of the bound vortices. Starting from a differential problem, the system is transformed into a set of simple algebraic equations in which the only unknown is the vortex strength. This system can be efficiently and rapidly solved using numerical techniques.

Once the vorticity distribution and velocities are determined, the calculation of aerodynamic loads can be performed using the theory of circulatory flows, specifically employing the Joukowski method. In this method, the contribution of a single vortex segment to the total aerodynamic load is computed as follows:

$$\delta\mathbf{F} = \rho\Gamma_{\delta l} (\mathbf{U} \times \delta\mathbf{l})$$

The lift and drag forces exerted by vortex segment are obtained by integrating induced the velocity caused by the segment over the surface of the plate. Induced velocity at any point on the plate can be determined by summing the contributions from all vortex segments using the Biot-Savart law.

To calculate the lift force, the component of the induced velocity perpendicular to the freestream direction is integrated over the plate surface. This accounts for the circulation generated by the vorticity distribution and results in the generation of lift. Similarly, the drag force is calculated by integrating the component of the induced velocity parallel to the freestream direction over the airfoil surface. This represents the drag generated by the vorticity distribution.

The theory of circulatory flows assumes that the flow is inviscid and incompressible, and it considers the circulation around the plate as the main source of aerodynamic forces. By evaluating the contributions from each vortex segment and summing them, the total lift and drag forces acting on the plate can be determined.

#### **4.4 MATLAB Implementations**

The initial step in the calculation involves determining the position of the wing based on the positions of its two corner points, considering the wing's rigid nature. The wing is then divided into panels according to the desired discretization. Once these initial steps are completed, the calculation of aerodynamic loads can be initiated. This involves computing the collocation point and determining the normal and tangential vectors for each vortex ring. Additionally, the panel areas are calculated. The most recent vortex ring is then shed into the wake.

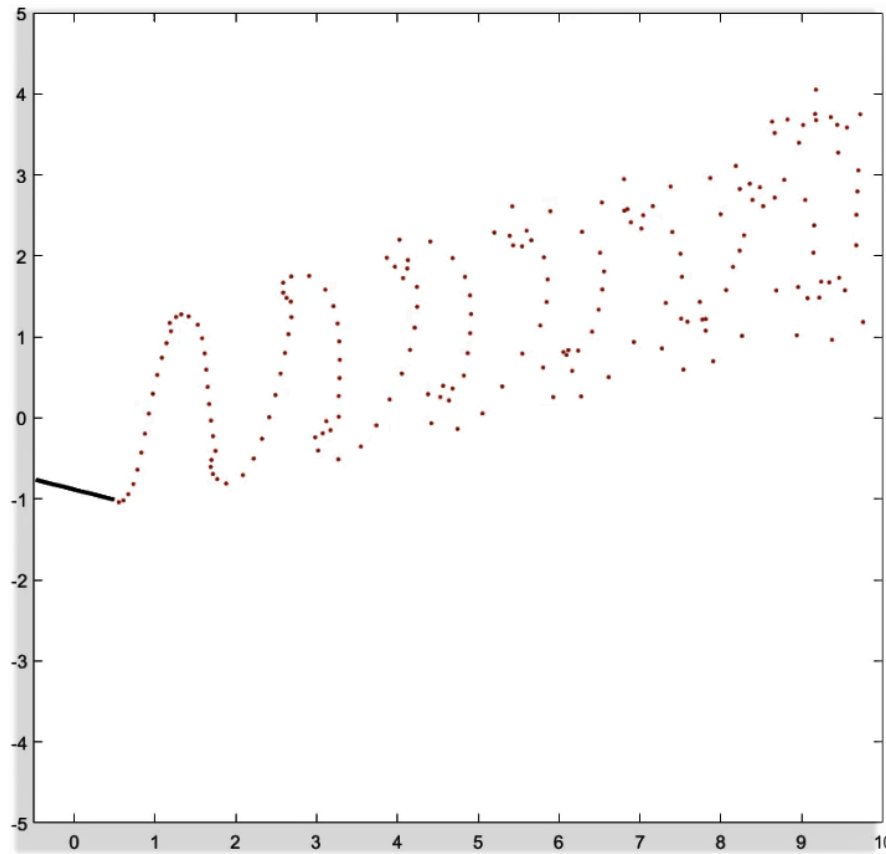


*Figure 10: Matlab Results*

The influence matrices can now be computed, and the external velocities are determined. By utilizing the wake vorticities from the previous time step, the induced velocities caused by the wake can be computed at the collocation points and the midpoints of each vortex segment (for the Joukowski method). This data enables the calculation of the bound vorticities by enforcing the impermeability condition at the collocation points. Finally, the velocities resulting from the wing vorticity are computed at collocation point defined for each vortex panel.

Once all the necessary calculations are completed, the determination of the aerodynamic loads can be addressed. In the case of the Joukowski method, the vortex filament vectors are determined using the corner points of the vortex ring. The total force components are then computed using the relevant equations. Notably, the local flow velocity used in the calculations is the flow velocity determined at the midpoint of the vortex segment, rather than at the collocation point.

Finally, the wake propagation is performed, and the positions of the wake corners are calculated based on the chosen wake model (flat or free wake). Figure 10 shows the position of wing and wake at 20-degree angle of attack. These steps are repeated for each time step until the specified number of periods is reached or until the wake has reached a sufficient length in steady cases. Once the loads are determined for each panel at each time step, the total forces acting on the entire wing can be computed for each time step.

## **4.5 Aerodynamic Loads**

Aerodynamics analysis of the flapping wing micro aerial vehicle using the unsteady vortex lattice method yielded insightful results. The analysis was conducted with a reduced frequency of 0.89 Hz, a pitch amplitude of 30 degrees, and a heave amplitude of 1 chord length. A free stream velocity of 1 m/s and an angle of attack of 20 degrees were specified for the analysis.

The results of the analysis provided important aerodynamic parameters, specifically the values of lift and thrust. By utilizing dimensionless parameters, the coefficients of lift and drag were calculated, resulting in a coefficient of lift of 1.537 and a coefficient of drag of -0.86. These results serve as a foundation for the subsequent design phase of the flapping wing micro aerial vehicle. The positive coefficient of lift signifies the ability of the wings to generate upward lift, supporting the weight of the vehicle. The negative coefficient of drag suggests that the wings produce forward thrust, enabling the vehicle to move through the air.

The obtained results validate the effectiveness of the unsteady vortex lattice method in predicting the aerodynamic behavior of the flapping wing micro aerial vehicle. In comparison to the numerical approach, analytical approach offers simplicity, computational efficiency, and allows for parametric study of the aerodynamic characteristics of the wing. With a thorough understanding of the aerodynamics of the flapping wing, we can now advance to the design stage of our mechanism. The findings in this section will guide the selection of optimal planform of the wing, its size, and orientation. Moreover, it would allow

optimization of other design parameters that would maximize lift, minimize drag, and enhance the overall flight performance of the micro aerial vehicle.

## **CHAPTER 5: DESIGN OF FLAPPING MECHANISM**

There is no specialized equipment to power the flapping wing motion, which is powered by a dc motor. Therefore, a mechanism is required to convert the rotational motion of the motor to the flapping motion of the wings. Different mechanisms have been used for this purpose, such as the slider-crank mechanism, single crank double rocker mechanism, and double-crank mechanism. All mechanisms consist of a rotating crank that is driven by the motor and a connecting rod, one end of which is attached to the crank and the other end to the wing. As the motor rotates the crank, the rotational motion of the crank is transmitted by the connecting rod, forcing the wing to move in up and down motion. In this way, the natural wing movement of birds and insects is mimicked, allowing the micro-UAV to have a flapping motion capable of generating lift and maintaining controlled flight. In the mechanism depicted in Figure 11, several parameters play important roles in its functionality. Let's delve further into each of these parameters:

## **5.1 Parameters**

The parameters associated with the mechanism play a vital role in determining its motion and functionality. Figure 11 provides an illustrative representation of the six-bar mechanism, highlighting labeled components such as the crank radius ( $R$ ), connecting rod length ( $L$ ), slider, connecting rod (length  $b$ ), and rocker (length  $a$ ). The crank radius influences the lever arm length and resulting motion, while the connecting rod length affects the reciprocating motion in the vertical direction. The slider crank mechanism converts the rotary motion of the crankshaft into vertical reciprocating motion, and the connecting rod transfers this motion to the rocker, enabling oscillating motion. By understanding and manipulating these parameters, a mechanism's performance can be enhanced and valuable insights can be gained into its behavior and dynamics.

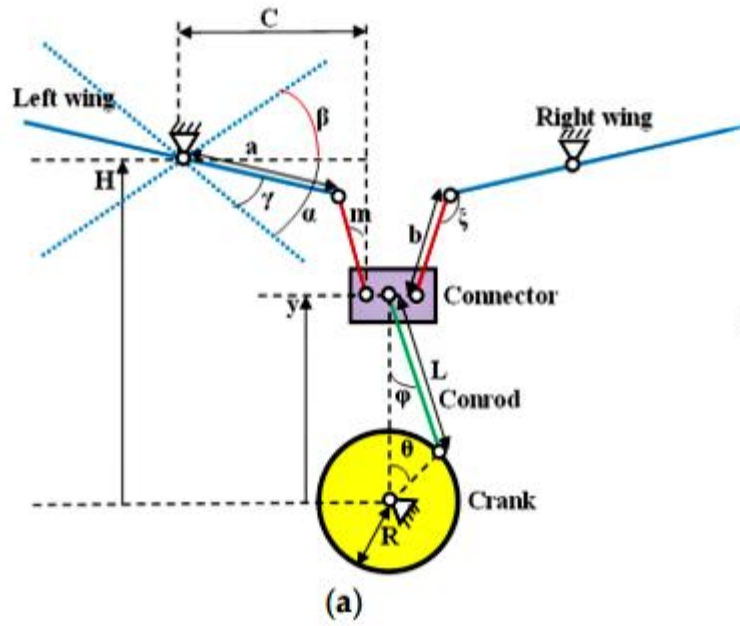


Figure 11: Slider Crank Mechanism

### 5.1.1 Radius of Crank (R)

The radius of the crank, denoted as  $R$ , represents the distance from the center of the crankshaft to the point where the connecting rod is attached. This parameter governs the smooth transmission of the rotational motion. By varying the radius of the crank, the mechanical advantage can be adjusted.

### 5.1.2 Length of Connecting Rod (L)

The length of the conrod, denoted as  $L$ , refers to the distance between the attachment point on the crank and the attachment point on the slider or connecting member. The conrod acts as a linkage between the crank and the slider crank mechanism. By changing the length of the conrod, the displacement and velocity of the slider can be modified, thereby affecting the reciprocating motion in the vertical direction.

### **5.1.3 Slider**

The connector member serves as a slider crank mechanism, which converts the rotary motion of the crankshaft into reciprocating motion in a vertical direction. It consists of a slider that moves along a fixed guide or track. The connector member's role is to transfer the motion generated by the crankshaft to the slider, producing the desired vertical reciprocating motion.

### **5.1.4 Connecting Rod (Length $b$ )**

The connecting rod, represented by  $b$  in length, is critical to the mechanism. It links the slider to the rocker and translates the connector member's reciprocating action into an oscillating motion in the rocker. The length of the connecting rod influences the amplitude and timing of the rocker's oscillating motion, which in turn influences the overall motion of the mechanism.

### **5.1.5 Rocker (Length $a$ )**

The rocker is the component that undergoes the oscillating motion required to produce flapping. It is made up of two sections, the first of which has a length equal to  $a$ . The connecting rod is attached to the rocker and transmits the sliding motion to the rocker's oscillating motion. While the second part is the part that extrudes after the fixed joint. The significance of the second part is to create a moment arm for the wing so can be of any desired length. The range and features of the oscillation are determined by the length of the initial section of the rocker length  $a$ ).

## **5.2 Derivation of the Position, Velocity and Acceleration**

To ensure the smooth operation of the mechanism it is crucial that the motion of connecting member is a harmonic motion. Otherwise, the motion would not be smooth and cause damage to the mechanism. For this reason, the  $L/R$  ratio should be selected carefully. However, increasing this dimensionless parameter will also increase the weight and size of the mechanism. So, it is very important to optimize this parameter for maximum efficiency during the design phase of the mechanism.

Considering the schematic presented in below Figure 12, the equations of the position, velocity, and acceleration of the connector member, respectively, are given by:

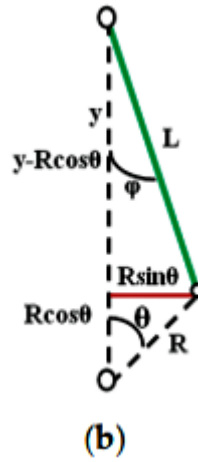


Figure 12: Mechanism Part I

$$L^2 - R^2 \sin^2(\theta) = (y - R \cos(\theta))^2$$

$$y - R \cos(\theta) = \sqrt{L^2 - R^2 \sin^2(\theta)}$$

The equation of position after rearranging the above equation is given as:

$$y = R \left( \sqrt{\left(\frac{L}{R}\right)^2 - \sin^2(\theta)} + \cos(\theta) \right)$$

Taking derivative of the above equation would give us the velocity:

$$\dot{y} = R\dot{\theta} \left( \frac{\cos(\theta) \sin(\theta)}{\sqrt{\left(\frac{L}{R}\right)^2 - \sin^2(\theta)}} - \sin(\theta) \right)$$

Similarly acceleration would be the derivative of above velocity:

$$\ddot{y} = -R\omega^2 \left( \frac{\cos(\theta)}{\left(\frac{L}{R}\right)^2 - \sin^2(\theta)} + \frac{\sin^2(2\theta)}{4 \left(\left(\frac{L}{R}\right)^2 - \sin^2(\theta)\right)^{3/2}} + \cos(\theta) \right)$$

Angular velocity is related to the frequency of oscillations by  $\omega = 2\pi f$ .

### **5.3 Derivation of the Flapping Angle and Angle of Transmission**

The flapping angle refers to the angle formed between the wings' position at their highest point (upstroke) and their lowest point (downstroke) during each flapping cycle. It represents the angular displacement or movement of the wings during the flapping motion of a micro-UAV. The transmission angle, in the context of mechanical systems, refers to the angle between the connecting rod and the line connecting the crankshaft center and the connecting rod center.

#### **5.3.1 Optimal Angle of Transmission:**

The optimal angle of transmission is an important factor in ensuring that power is efficiently transmitted to the flapping wings. This angle is calculated by taking into account several aspects, such as the design of the connecting rod, the form and size of the crank, and the required flying characteristics. The optimal angle of transmission aims to minimize energy losses and maximize the conversion of rotational motion into the desired reciprocating motion. By finding the optimal angle, the flapping mechanism can achieve the highest level of efficiency and effectiveness in generating lift and thrust. To determine the optimal angle of transmission, the angle of intersection of the members needs to be calculated both analytically and through computer simulations. In this way, optimal configuration is identified that has the best overall performance and meets the design objectives of the micro-UAV.

Subsequently, we establish the connections between the flapping angle ( $\gamma$ ), the angular position of the crank ( $\theta$ ), and various other factors that influence the flapping angle.

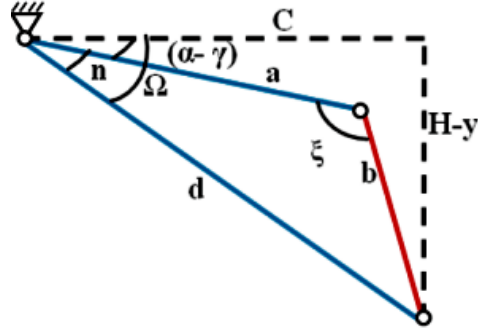


Figure 13: Mechanism Part II

From the above figure:

$$H = y + b \cos(m) + a \sin(\alpha - \gamma)$$

$$b^2 = (b \cos(m))^2 + (c - a \cos(\alpha - \gamma))^2$$

$$\cos(m) = \sqrt{1 - \left(\frac{c - a \cos(\alpha - \gamma)}{b}\right)^2}$$

Substitute  $\cos(m)$  and "y" in the equation.

$$H = R \left( \sqrt{\left(\frac{L}{R}\right)^2 - \sin^2(\theta)} \right) + b \sqrt{1 - \left(\frac{c - a \cos(\alpha - \gamma)}{b}\right)^2} + a \sin(\alpha - \gamma)$$

Where "H" represents the constant-length distance between the origin and the point of wing pivot. Now using the law of sines, the angle n can be expressed as:

$$\frac{\sin(n)}{b} = \frac{\sin(\epsilon)}{d} \rightarrow n = \arcsin\left(\frac{b \sin(\epsilon)}{a}\right)$$

$$d = \sqrt{c^2 + (H - y)^2} = \sqrt{c^2 + \left[ H - R \left( \sqrt{c^2 - \sin^2(\theta)} + \cos(\theta) \right) \right]^2}$$

According to the above equations of “d”, the transmission angle ( $\xi$ ) can be expressed as:

$$\epsilon = \arccos\left(\frac{\left[H - R\left(\sqrt{c^2 - \sin^2(\theta)} + \cos(\theta)\right)\right]^2 + c^2 - a^2 - b^2}{-2ab}\right)$$

### 5.3.2 Flapping Angle:

The flapping angle is a fundamental parameter in the design and operation of flapping-wing systems. It directly influences the aerodynamic forces generated by the wings during flight. By varying the flapping angle, the micro-UAV can control the magnitude and direction of lift and thrust. For example, a larger flapping angle can generate more lift but may also increase drag. On the other hand, a smaller flapping angle reduces lift but enhances maneuverability. The flapping angle can be adjusted by altering the design of the flapping mechanism, wing structure, or control system to optimize the flight performance based on the specific requirements of the micro-UAV.

Now for flapping angle “ $\gamma$ ”, we can write the below equation

$$(\alpha - \gamma) = \psi - n$$

Substitute below equations in the above equation:

$$\psi = \arctan\left(\frac{H - y}{C}\right)$$

Equation of position “ $y$ ” is now given as:

$$y = R\left(\sqrt{\left(\frac{L}{12}\right)^2 - \sin^2(\theta)}\right) + \cos(\theta)$$

Angle  $n$  can now be expressed using the law of sine:

$$n = \arcsin\left(\frac{b \sin(\epsilon)}{a}\right)$$

From all the above equations flapping angle will be:

$$\gamma = -\arctan\left(\frac{H - R\left(\sqrt{(c)^2 - \sin^2(\theta)}\right) + \cos(\theta)}{C}\right) + \arcsin\left(\frac{b \sin(\epsilon)}{a}\right) + \alpha$$

### 5.3.3 Design Parameters Calculation:

To perform the computations presented in the Table 3, several iterations were performed using the specified parameters. Each parameter has its own definition and function, and iterations were required to achieve the desired results. Let's go over the calculations and explain why each repetition is necessary:

- L (mm): This value represents the length and was set to 32 mm for all modes. This parameter did not require any iteration.
- R (mm): The radius parameter was likewise kept constant at 8 mm for all modes. No iteration was necessary for the length.
- a (mm): This variable value was altered in each mode. Iterations were carried out by gradually changing the value of "a" to see how it affected the subsequent calculations. By changing "a" several design situations can be investigated.
- b (mm): As with "a" the parameter "b" was changed in each mode to see how it affected the subsequent calculations. Small increments were made to the value of "b" in each iteration.
- L/R: The "L" to "R" ratio was calculated by dividing the length by the radius. Different values of L/R were initially checked to see if the motion of slider was harmonic. Once the ratio came out as 4, no changes were deemed necessary for rest of the iterations.
- H (mm): For all modes, the height parameter "H" remained constant at 46 mm. There was no need for iteration.
- $\gamma_{\max}$ : This value was calculated using a specific formula based on the given

parameters and their relationships. Iterations were carried out to investigate the variation in " $\gamma_{\max}$ " for various parameter combinations.

- $\gamma_{\min}$ : Like " $\gamma_{\max}$ ," the value of " $\gamma_{\min}$ " was determined based on the factors and their relationships. Iterations were performed to assess the effect of parameter modifications on " $\gamma_{\min}$ ."
- $\gamma_{\max} - \gamma_{\min}$ : This calculation involved subtracting the value of "Ymin" from the value of "Ymax" to obtain the difference. The value of "Ymax" and "Ymin" should correspond to values of " $\epsilon_{\max}$ " and " $\epsilon_{\min}$ ".
- $\epsilon_{\max}$ : The value of " $\epsilon_{\max}$ " was calculated using a specific formula or formulas based on the parameters. Iterations were carried out to evaluate the effect of parameter modifications on " $\epsilon_{\max}$ ".
- $\epsilon_{\min}$ : Like " $\epsilon_{\max}$ ," the value of " $\epsilon_{\min}$ " was determined using a formula or calculation based on the parameters provided.- Iterations were performed to assess the impact of parameter changes on " $\epsilon_{\min}$ ."
- $\epsilon_{\max} - \epsilon_{\min}$ : This calculation included subtracting the value of " $\epsilon_{\min}$ " from the value of " $\epsilon_{\max}$ " to obtain the difference. Result was compared with the value of "Ymax" and "Ymin".

Parameter	Model 1	Model 2	Model 3	Model 4	Model 5
L (mm)	32	32	32	32	32
R (mm)	8	8	8	8	8
a (mm)	15	14	13.5	13	12.5
b (mm)	17	17	15.5	15	14.5
L/R	4	4	4	4	4
H (mm)	46	46	46	46	46
C (mm)	15	15	13.5	13	12.5
$\gamma_{\max}$ (°)	84.2	86.4	82.3	81.6	80.9

$\gamma_{\min}$ (°)	20.4	18.6	10.8	6.6	1.7
$\gamma_{\max} - \gamma_{\min}$ (°)	63.8	67.8	71.5	75	79.2
$\epsilon_{\max}$ (°)	112.5	118.1	125.6	131.6	139
$\epsilon_{\min}$ (°)	60.3	61.9	60.8	61	61.3
$\epsilon_{\max} - \epsilon_{\min}$ (°)	52.2	56.2	64.8	70.6	77.7

Table 3: Parameter Values

Overall, the iterations were carried out to investigate the interactions between different factors and to comprehend how changes in one parameter influenced subsequent calculations. It was feasible to obtain insights into the design characteristics and make educated decisions based on the desired objectives by analysing the results of each iteration.

## 5.4 Mechanism Design on Solidworks

Using the determined length of the rod (L), SolidWorks facilitated the creation of a 3D model that accurately represented the physical dimensions of the rod. By inputting the calculated values for the radius of the crank (R), connecting rod length (b), rocker length (a), distance between the origin and wing pivot (H), and the horizontal length from wing pivot to slider connector (C), SolidWorks enabled the assembly of the mechanism with the correct dimensions and relationships between the components.

Furthermore, SolidWorks provided simulation capabilities to analyze the mechanism's performance based on the calculated parameters. By considering the maximum and minimum flapping angles ( $\gamma_{\max}$  and  $\gamma_{\min}$ ) and transmission angles ( $\epsilon_{\max}$  and  $\epsilon_{\min}$ ), designers could simulate and evaluate the motion and functionality of the mechanism. SolidWorks motion analysis tools allowed for the verification of the range of motion of the flapping wings and the transmission angles, ensuring they aligned with the desired design goals.

SolidWorks optimization features could also be leveraged to refine the mechanism's performance based on the calculated parameters. Designers could adjust the parameters such as the lengths of the rod, crank, connecting rod, rocker, and distances between components to

achieve optimal efficiency, motion characteristics, and power transmission within the mechanism.

#### 5.4.1 Prototype I

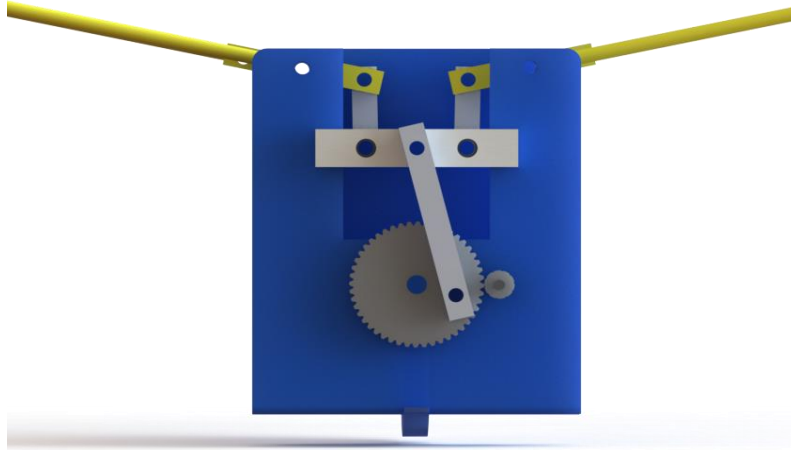


*Figure 14: Prototype I*

The first prototype, as shown in Figure 14, was designed to keep gear ratio of 48:10 and parameter values of model 4 listed in Table 3. The prototype had a slider to ensure stable flapping of wing rods. After fabrication by 3D printing using PLA material, it was found that slider friction with contacting surface decreased link velocity and increased temperature. This defect along with the high prototype weight rendered it useless for the final product.

#### 5.4.2 Prototype II

The second prototype, as shown in Figure 15, was designed by further optimizing the mechanism parameters and using those of 5<sup>th</sup> Model. The gear ratio was kept same but the slider was removed. This gave reasonable results that could be used for designing the final product. Thus, this design was finalized.

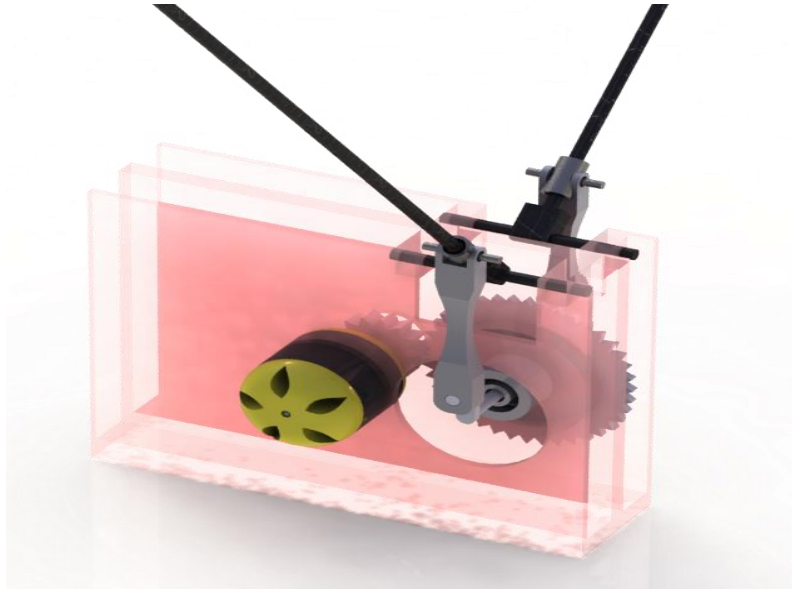


Figure 15: Prototype II

## 5.5 Design Validation by Fabrication

After the completion of the preceding steps which included Kinematic parameter extraction from highspeed camera video, developing equations on those parameters, designing a mechanism governed by those equations and performing aerodynamics analysis, we proceeded with fabricating the mechanism and developing a MAV. The parameters decided for the fabrication were as given in the table below:

Parameters	Values
Wingspan	50 cm
Frequency	8 Hz
Amplitude	23 cm
Design Velocity	3 m/s
Design Weight	67 g

Table 4: Design Parameters

## CHAPTER 6: RESULTS

In the video analysis and kinematics section, parameters such as flapping angles, phase angles, and angle of attack were measured using advanced computer vision techniques and tracking algorithms. These measurements provided valuable insights into the kinematics of dragonfly flight, contributing to our understanding of flight dynamics, maneuverability, and aerodynamic performance. The derived kinematic equations accurately described the intricate wing motion, further enhancing our comprehension of the aerodynamic forces and lift generation exhibited by dragonflies. These results serve as a solid foundation for MAV design and optimization, guiding the development of MAVs that mimic the flight capabilities of dragonflies.

### 6.1 Flight Data

The analysis of the mapped coordinates of the dragonfly's wings yielded important findings. The calculated values for the flap angle ranged from  $35^\circ$  to  $-33^\circ$ , indicating the range of angular displacement exhibited by the wings during the flapping motion. Similarly, the angle of attack values ranged from  $30^\circ$  to  $-21^\circ$ , providing insights into the orientation of the wings with respect to the relative airflow direction during flight. Important parameters have been summarized in Table 5.

Parameter	Measurement
Body Length (mm)	$34.5 \pm 0.1$
Forewing Length (mm)	$32.5 \pm 0.1$
Flapping Frequency (Hz)	$25 \pm 1$
Flap Angle ( $^\circ$ )	$35^\circ$ to $-33^\circ$
Angle of Attack ( $^\circ$ )	$30^\circ$ to $-21^\circ$
Phase Angle ( $^\circ$ )	$60^\circ \pm 1$

Table 5: Flight Data

Furthermore, from the calculations of flap angle, angle of attack, and phase angle, sinusoidal waveforms representing the motion of the dragonfly's flapping wings were derived as shown in Figure 16. These waveforms, obtained through careful analysis of the angle measurements, offer valuable information for modeling the pitch and heave motions of the wings. The heave motion, which describes the up-and-down movement of the wings, can be accurately described by the equation  $h(t) = h_0 \cos(2\pi ft)$ , where  $h(t)$  represents the heave displacement at time  $t$ ,  $h_0$  is the amplitude of the heave motion,  $f$  is the wingbeat frequency, and  $t$  is time. The cosine function generates a wave that oscillates between positive and negative values, capturing the cyclical nature of the pitch motion.

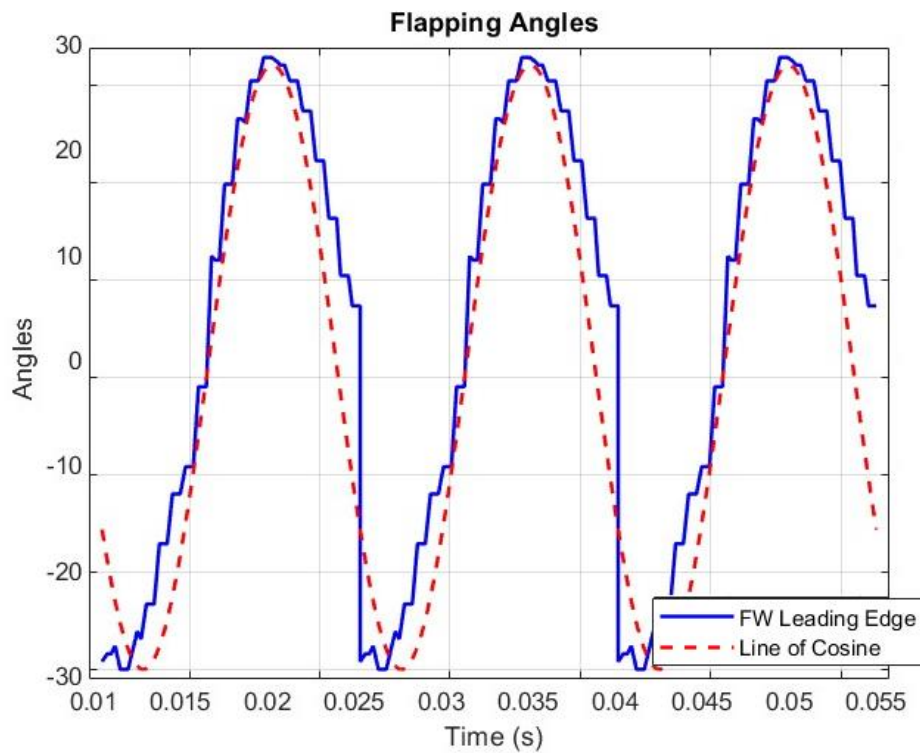


Figure 16: Flapping Angle

Similarly, the pitch motion, representing the rotation of the wings, can be described by the equation  $\Phi(t) = \Phi_0 \sin(2\pi ft)$ , where  $\Phi(t)$  represents the pitch displacement at time  $t$ ,  $\Phi_0$  is the pitch amplitude,  $f$  is the wingbeat frequency, and  $t$  is time. The sine function generates a waveform that oscillates between positive and negative values, capturing the periodic back-and-forth motion of the wings.

These governing equations provide a mathematical representation of the pitch and heave motions of the dragonfly's wings during flight. They enable quantitative analysis and modeling of the complex wing kinematics, facilitating a deeper understanding of the aerodynamic forces, lift generation, and maneuverability exhibited by the dragonfly.

## 6.2 Factors Affecting Lift Coefficient

The mean angle of attack and flapping frequency are critical parameters in the design of a flapping wing mechanism. Figure 17 shows values of the coefficient of lift for different reduced frequencies and mean angle of attack ( $\theta_m = 0^\circ, 10^\circ$  and  $20^\circ$ ). It can be observed that at  $\theta_m = 0^\circ$ , lift coefficient is zero. As  $\theta_m$  is increased the value of coefficient of lift also increases with the greatest lift coefficient observed when  $\theta_m = 20^\circ$ . However, it is important to note that at greater angles of attack, the wings may stall at local angles of attack, which can negatively impact flight performance. In addition to the mean angle of attack, the flapping frequency also plays a significant role in determining flight performance. As the flapping frequency increases, lift coefficient also increases. This suggests that by varying both the mean angle of attack and the flapping frequency during flight, it may be possible to optimize the lift and improve the overall flight performance.

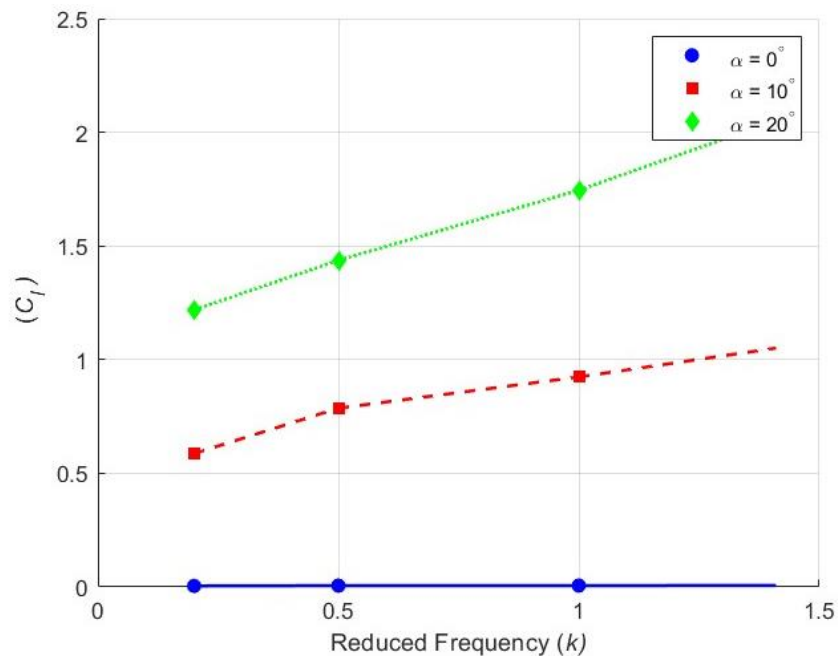


Figure 17: Coefficient of Lift

During the design process of a flapping wing mechanism, it is crucial to carefully consider the parameters that affect flight performance, such as the mean angle of attack and flapping frequency. Once the mechanism has been designed, these parameters can be controlled during flight using a remote controller. For example, the mean angle of attack can be varied by adjusting the elevator, allowing the pilot to optimize lift and improve flight performance. Similarly, the flapping frequency can be controlled by adjusting the rpms of the motor that drives the flapping mechanism. By carefully adjusting the motor rpms, the pilot can increase or decrease the flapping frequency to optimize the lift and improve the flight performance. In summary, by carefully controlling these parameters, pilots can make real-time adjustments to the flight path making it possible to achieve stable and efficient flight with precise control over the flight trajectory.

### **6.3 Force Coefficients**

The aerodynamics analysis of the flapping wing micro aerial vehicle using the unsteady vortex lattice method has yielded insightful results. The analysis was performed with specific parameters: a reduced frequency of 0.89 Hz, a pitch amplitude of 30 degrees, and a heave amplitude of 1 chord length. Additionally, a free stream velocity of 1 m/s and an angle of attack of 20 degrees were specified for the analysis. The results of the analysis provided values of lift and thrust. By employing dimensionless parameters, the coefficients of lift and drag were calculated, yielding a coefficient of lift of 1.537 and a coefficient of drag of -0.86, as shown in Figure 17 and 18 respectively.

The positive coefficient of lift indicates the ability of the wings to generate upward lift, effectively supporting the weight of the vehicle. This finding suggests that the wings possess the necessary aerodynamic characteristics to provide the necessary lift for sustained flight. Furthermore, the negative coefficient of drag indicates that the wings are capable of producing forward thrust, enabling the vehicle to move through the air efficiently. The positive lift coefficient and negative drag coefficient affirm the feasibility of utilizing flapping wing mechanisms to achieve controlled flight. This information is pivotal in guiding the subsequent design and optimization stages of the micro aerial vehicle, facilitating the

development of efficient and maneuverable systems that can mimic the flight capabilities of insects.

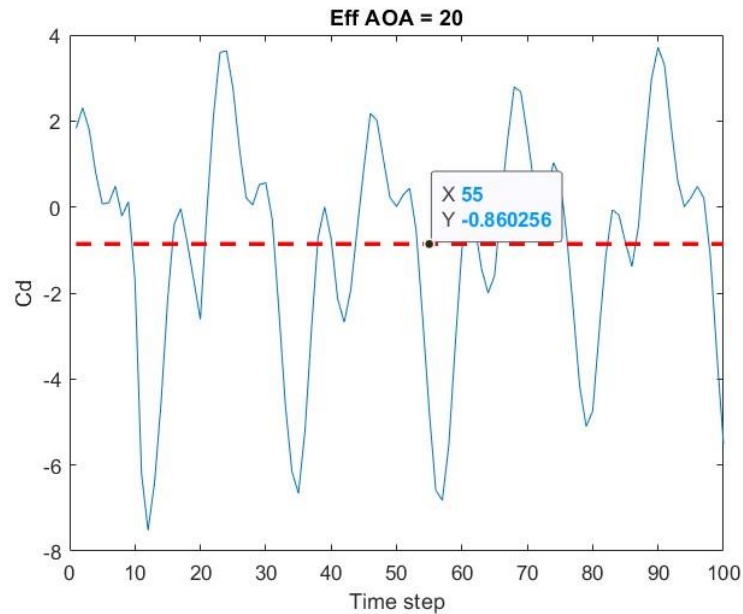


Figure 18: Coefficient of Drag

## 6.4 Flight Performance

The examination of aerodynamic forces such as lift, thrust, and drag, offers valuable insights into the flight performance of MAVs. These forces play a pivotal role in determining the MAV's ability to achieve sustained and controlled flight. Notably, aerodynamic forces exhibit a direct proportionality to the square of the vehicle's velocity, as confirmed by the trends depicted in Figure 19. This relationship underscores the significance of velocity in influencing the magnitude of these forces.

At lower velocities, a higher level of drag is observed, indicating increased resistance experienced by the MAV. However, as the MAV is imparted with an initial push and its velocity increases, it overcomes the drag and attains desirable flight characteristics. This is evidenced by comparing the thrust and drag values at different velocities, where it becomes apparent that the thrust exceeds the drag, indicating good flight performance of the MAV.

It is important to acknowledge that the evaluation considers only the induced and form drag components. In reality, the total drag experienced by the MAV should increase and eventually equal the thrust, reaching a point where the vehicle would move at a constant speed. It is also worth noting that the coefficient of thrust decreases with increasing speed. This trend can be attributed to the increased drag experienced by the MAV's wings as the velocity rises. The increasing drag puts a constraint on the MAV's ability to generate forward thrust efficiently.

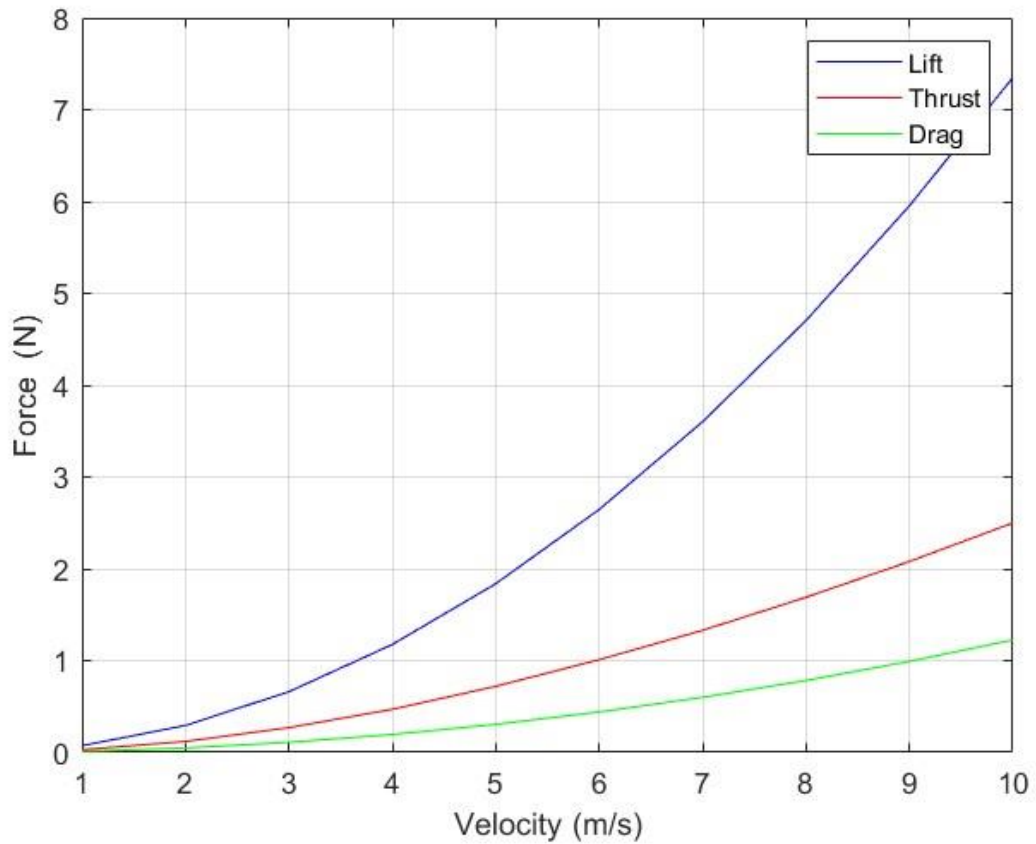


Figure 19: Flight Performance

## CHAPTER 7: CONCLUSION

This paper presents the design and development of a dragonfly-inspired robot, with a focus on extracting and analyzing dragonfly flight kinematics. To extract the kinematics of dragonfly flight, a Python code was developed that allowed tracking of wing motion. After extracting the kinematics of a dragonfly, various kinematic and kinetic analyses were performed, leading to the development of a methodology that relates optimal parameters of the actuation mechanism to the input parameters such as upstroke and downstroke angles and flapping frequency. The developed methodology demonstrates the feasibility of designing an efficient slider-crank actuation mechanism with symmetrical flapping motion. This designed mechanism consisting of six-bar mechanism was successfully manufactured. Two prototypes of the dragonfly robot equipped with a single pair of wings, driven by DC motors were designed. The final prototype achieved a wingspan of 50 cm and a wingbeat frequency of up to 10 Hz. With a total weight of 57 grams (including batteries and electronics), the mechanism remains within the designated design parameters, indicating its potential for sustainable flights.

However, it is important to note that further optimizations are required to achieve higher wingbeat frequencies and generate sufficient lift. Additional design refinements are necessary to address these challenges. Furthermore, as part of the long-term objectives of this prototype development, efforts are underway to implement dynamic variable phase differences during flight.

These findings contribute to the field of biomimetic robotics by providing insights into the design and development of flapping wing mechanisms inspired by dragonflies. The research highlights the potential of leveraging the unique characteristics of dragonfly flight to create agile and efficient robotic systems. The outcomes of this study lay the groundwork for future advancements and improvements in dragonfly-inspired robot prototypes, with the ultimate goal of achieving dynamic flight capabilities.

## REFERENCES

- [1] Azuma, A., Azuma, S., Watanabe, I., Furuta, T.: Flight mechanics of a dragonfly. *J. Exp. Biol.* 116, 79–107 (1985)
- [2] May, M.L.: Dragonfly flight: power requirement at high speed and acceleration. *J. Exp. Biol.* 158, 325–342 (1991)
- [3] Wakeling, J.M., Ellington, C.P.: Dragonfly flight. I. Gliding flight and steady-state aerodynamic forces. *J. Exp. Biol.* 200, 543–556 (1997)
- [4] Freymuth, P.: Thrust generation by an airfoil in hover modes. *Exp. Fluids* 9, 17–24 (1990)
- [5] Thomas, A.L., Taylor, G.K., Srygley, R.B., Nudds, R.L., Bompfrey, R.J.: Dragonfly flight: free-flight and tethered flow visualizations reveal a diverse array of unsteady lift-generating mechanisms, controlled primarily via angle of attack. *J. Exp. Biol.* 207, 4299–4323 (2004)
- [6] Wang, Z.J.: Vortex shedding and frequency selection in flapping flight. *J. Fluid Mech.* 410, 323–341 (2000)
- [7] Wu, J.H., Sun, M.: Unsteady aerodynamic forces of a flapping wing. *J. Exp. Biol.* 207, 1137–1150 (2004)
- [8] Wang, Z.J.: Dissecting insect flight. *Ann. Rev. Fluid Mech.* 37, 183–210 (2005)
- [9] Weis-Fogh T. Quick estimates of flight fitness in hovering animals, including novel mechanisms for lift production. *J Exp Biol* 1973; 59: 169–230.
- [10] Bode-Oke AT, Zeyghami S, Dong H. 2018 Flying in reverse: kinematics and aerodynamics of a dragonfly in backward free flight. *J. R. Soc. Interface* 15: 20180102.

- [11] G Ruppell. Kinematic analysis of symmetrical flight maneuvers of odonata. *Journal of Experimental Biology*, 144(1):13–42, 1989.
- [12] Chengyu Li and Haibo Dong. Wing kinematics measurement and aerodynamics of a dragonfly in turning flight. *Bioinspiration & Biomimetics*, 12(2), 2017.
- [13] CP Ellington. The aerodynamics of hovering insect flight. iv. aerodynamic mechanisms. *Philosophical Transactions of the Royal Society of London. B, Biological Sciences*, 305(1122):79–113, 1984.
- [14] James M Birch and Michael H Dickinson. Spanwise flow and the attachment of the leading-edge vortex on insect wings. *Nature*, 412(6848):729–733, 2001.
- [15] Timothy M Broering, Yongsheng Lian, and William Henshaw. Numerical investigation of energy extraction in a tandem flapping wing configuration. *AIAA Journal*, 50(11):2295–2307, 2012
- [16] Simon M Walker, Adrian LR Thomas, and Graham K Taylor. Photogrammetric reconstruction of high-resolution surface topographies and deformable wing kinematics of tethered locusts and free-flying hoverflies. *Journal of The Royal Society Interface*, 6(33):351–366, 2009.
- [17] Simon M Walker, Adrian LR Thomas, and Graham K Taylor. Photogrammetric reconstruction of high-resolution surface topographies and deformable wing kinematics of tethered locusts and free-flying hoverflies. *Journal of The Royal Society Interface*, 6(33):351–366, 2009.
- [18] AC Carruthers, SM Walker, ALR Thomas, and GK Taylor. Aerodynamics of aerofoil sections measured on a free-flying bird. *Proceedings of the Institution of Mechanical Engineers, Part G: Journal of Aerospace Engineering*, 224(8):855– 864, 2010.
- [19] Fritz-Olaf Lehmann. The mechanisms of lift enhancement in insect flight. *Naturwissenschaften*, 91(3):101–122, 2004
- [20] Diana D Chin and David Lentink. Flapping wing aerodynamics: from insects to vertebrates. *Journal of Experimental Biology*, 219(7):920–932, 2016.

[21] David E Alexander. Unusual phase relationships between the forewings and hindwings in flying dragonflies. *Journal of Experimental Biology*, 109(1):379– 383, 1984.

---